Journal: *Agricultural and Forest Meteorology*

Title: Dynamic biotic controls of leaf thermoregulation across the diel timescale

Author List: Zhengfei Guo[1], Zhengbing Yan[1], Bartosz Marek Majcher[1], Calvin K. F. Lee[1], Yingyi Zhao[1], Guangqin Song[1], Bin Wang[2,3], Xin Wang[2,3], Yun Deng[3,4,5], Sean T. Michaletz[6], Youngryel Ryu[7], Louise Amy Ashton[1], Hon-Ming Lam[8], Man Sing Wong[9], Lingli Liu[2,3], and Jin Wu[1,10*]

Author Affiliations:

(1) School of Biological Sciences, The University of Hong Kong, Pokfulam, Hong Kong SAR, China

(2) State Key Laboratory of Vegetation and Environmental Change, Institute of Botany, Chinese Academy of Sciences, Xiangshan, Beijing, China

(3) The University of Chinese Academy of Sciences, Yuquan Road, Beijing, China

(4) CAS Key Laboratory of Tropical Forest Ecology, Xishuangbanna Tropical Botanical Garden, Chinese Academy of Sciences, Menglun, Mengla, Yunnan 666303, China

(5) National Forest Ecosystem Research Station at Xishuangbanna, Xishuangbanna Tropical Botanical Garden, Chinese Academy of Sciences, Menglun, Mengla, Yunnan 666303, China

(6) Department of Botany and Biodiversity Research Centre, University of British Columbia, Vancouver, BC, Canada

(7) Department of Landscape Architecture and Rural Systems Engineering, Seoul National University, South Korea

(8) Center for Soybean Research of the State Key Laboratory of Agrobiotechnology and School of Life Sciences, The Chinese University of Hong Kong, Shatin, Hong Kong SAR, China

(9) Department of Land Surveying and Geo-Informatics, The Hong Kong Polytechnic University, Hung Hom, Hong Kong SAR, China

(10) State Key Laboratory of Agrobiotechnology, The Chinese University of Hong Kong, Shatin, Hong Kong SAR, China

*** Corresponding Author:** Jin Wu

School of Biological Sciences, The University of Hong Kong, Pokfulam, Hong Kong SAR, China (email: jinwu@hku.hk; phone: +852 2299-0655)

Abstract

Leaf thermoregulation and consequent leaf-to-air temperature difference (ΔT) are tightly linked to plant metabolic rates and health. Current knowledge mainly focus on the regulation of environmental conditions on ΔT, while an accurate assessment of biotic regulations with field data remains lacking. Here, we used a trait-based model that integrates a coupled photosynthesis-stomatal conductance model with a leaf energy balance model to explore how six leaf traits (i.e. leaf width, emissivity, visible and near-infrared light absorptance, photosynthetic capacity—$V_{c,max25}$, and stomatal slope—g_1) regulate ΔT variability across the diel timescale. We evaluated the model with field observations collected from temperate to tropical forests. Our results show that: (1) leaf traits mediate large ΔT variability, with the noon-time trait-mediated ΔT variability reaching *c.* 15.0 °C; (2) leaf width, $V_{c,max25}$, and g_1 are the three most important traits and their relative importance in ΔT regulation varies strongly across the diel timescale; and (3) model-derived trait-ΔT relationships match field observations that were collected close to either midday or midnight. These findings advance our understanding of biotic controls of leaf-level ΔT variability, highlighting a trait-based representation of leaf energy balance that can improve simulations of diverse leaf thermoregulation strategies across species and physiological responses to climate change.

Keywords: leaf-to-air temperature difference, plant functional traits, leaf energy balance, coupled photosynthesis-stomatal conductance model, trait-based modeling, global sensitivity analysis

1. Introduction

Leaf temperature is tightly connected with vegetative functioning at all spatial scales, from individual plants to forest ecosystems. At the individual level, leaf temperature regulates plant ecophysiology through both direct controls on photosynthetic metabolism (Farquhar *et al.*, 1980; Bernacchi *et al.*, 2013) and indirect controls via temperature-associated leaf-to-air vapour pressure deficit (VPD_{leaf}) that down-regulates stomatal conductance (Lloyd & Farquhar, 2008). At the ecosystem level, leaf temperature is a key state variable of terrestrial biosphere models (TBMs), influencing large-scale biogeochemical cycles and vegetation-climate interactions (Best *et al.*, 2011; Bonan *et al.*, 2014; Smith *et al.*, 2020). Despite its importance, leaf temperature has long been approximated using air temperature (Helliker & Richter, 2008; Huang *et al.*, 2019). However, increasing field-based evidence challenges this approximation by showing that leaf-to-air temperature difference (ΔT) is considerable and has a highly dynamic nature (Leuzinger & Körner, 2007; Aubrecht *et al.*, 2016; Still *et al.*, 2019). Such temperature differences reflect that plants can thermoregulate to decouple their tissue temperature from the ambient air temperature, which suggests that approximating leaf temperature with air temperature could result in large uncertainties in TBMs for simulating terrestrial ecosystem response to climate change (Michaletz *et al.*, 2015; Dong *et al.*, 2017). Therefore, an improved understanding of leaf temperature and associated mechanistic controls of ΔT variations remains a central issue in many ecology-related disciplines, with increasing urgency under recent climate change.

Two approaches have been used to study leaf temperature and ΔT. One is based on a leaf energy balance model (Gates, 1968; Campbell & Norman, 2012). Since this approach has a strong theoretical basis, it has been widely implemented in TBMs to infer leaf temperature and simulate terrestrial ecosystem physiological response to climate variability (Bonan *et al.*,

2014; Lawrence *et al.*, 2018). Despite successful implementation in TBMs, there remain some important but understudied parameters in this modeling framework that correspond to key leaf traits. Energy balance equations usually contain multiple trait parameters, most of which are time-consuming to measure at a level and resolution associated with each leaf of interest (Jones, 2013; Michaletz *et al.*, 2016). For example, the measurements of stomatal slope and leaf absorptance, require specialised equipment and often take relatively long times to complete for a single tree, even when coordinated by a team (Wu *et al*., 2019, 2020). For simplicity's sake, they are often assigned with fixed values for each plant functional type in TBMs, without considering the potential large trait variability within and across vegetation biomes (e.g. Lin *et al.*, 2015; Wright *et al.*, 2017; Ivanova *et al.*, 2018). Consequently, this coarse characterization of leaf traits has caused inaccurate predictions for leaf temperature (Dong *et al*., 2017) and vegetation response to climate change (Rogers *et al*., 2017; Bonan & Doney, 2018).

The other commonly-used approach is statistically examining the relationships of ΔT with leaf traits. For example, leaf width has been shown to have a tight negative correlation with ΔT (Lusk *et al.*, 2018). The relationships between ΔT and several other leaf traits and processes have also been explored, including but not limited to leaf thickness (Leigh *et al.*, 2012), margin complexity (Leigh *et al.*, 2017), stomatal conductance (Leuzinger & Körner, 2007), and boundary layer resistance (Majcher, 2018). Compared with the leaf energy balance modeling approach, the statistical approach is advantageous in exploring the relationships of ΔT with specific traits in regulating ΔT dynamics at the finer scale (Jones, 1999; Økland, 2007). However, it has been criticized for being semi-empirical and lack of rigorous theoretical basis.

As the known trait-Δ*T* relationships remain limited to the easier-to-measure leaf traits listed above, other important but relatively difficult-to-measure traits remain underexplored. Take leaf maximum carboxylation capacity scaled to 25°C ($V_{c,max25}$) and Medlyn-type stomatal slope (g_1) as examples. They are two traits tightly connected with stomatal behaviors, and thus importantly regulate plant photosynthesis and transpiration rates (Medlyn *et al.*, 2011; Wu *et al.*, 2017, 2020). Despite this, how they affect Δ*T* is still not fully understood. Additionally, most relevant studies were conducted for a single time of the day, such as noon-time (Yu *et al.*, 2015) or midnight (Lusk *et al.*, 2018), though we expect these 'static' traits, like $V_{c,max25}$ and g_1, to have variable roles on their control of leaf temperature on a diel timescale. This is because although these traits remain constant throughout the day, the energy fluxes regulated by these traits, like latent heat and sensible heat, change (Jones, 2013; Still *et al.*, 2019), and may ultimately lead to a diel dynamic effect on Δ*T*. As such, we can infer that the trait-Δ*T* relationships derived from a single time may be misleading when applied to other periods of a day. All these limitations result in an incomplete understanding of how biotic factors, particularly multiple associated leaf traits, regulate Δ*T* variability (Dong *et al.*, 2017; Still *et al.*, 2019).

Integrating the leaf energy balance model with the plant physiology model may offer a solution to mechanistically assess how key leaf traits regulate Δ*T* variability via fundamental pathways (Fig. 1). This integration has been previously used in TBMs to explore and predict vegetation-atmosphere interactions (e.g. community land model—CLM 4.5 and 5.0; Oleson et al., 2010; Lawrence et al., 2018), but they are rarely evaluated with comprehensive field data (Dong *et al.*, 2017; Rogers *et al.*, 2017). This is because evaluation requires simultaneous measurements of environmental conditions and leaf physiological traits, which are labor-intensive and challenging to measure, especially for tall canopy trees (Wu *et al.*,

2019, 2020). Additionally, difficulties in trait measurements can hinder the accurate parameterization of TBMs (Rogers *et al*., 2017). A better strategy for model evaluation might be spending effort on the key leaf traits that are more important in leaf temperature regulation, while setting less-important traits as constants or approximations, simplifying the model constraints while ensuring model accuracy. Therefore, it is important to understand which traits dominate leaf temperature regulation.

This study aims to develop an improved understanding of biotic controls on ΔT variability. Specifically, we address three questions: (i) To what extent can leaf traits affect ΔT? (ii) What are the most important traits that regulate ΔT variability, and how do their relative roles vary at the diel timescale? (iii) Do trait-ΔT relationships based on our coupled model that integrates the leaf energy balance model with the plant physiology model agree with field observations? To address these questions, we used a trait-based leaf energy balance model, consistent with those implemented in TBMs, and a dataset with traits and ΔT collected from three distinct types of forests, including a temperate forest, tropical rainforest, and tropical dry forest. With this integrated model and field dataset, we hope to improve the mechanistic understanding of trait-ΔT relationships across both temporal (i.e. diel) and spatial (i.e. leaf samples within and across forest sites) scales.

2. Materials and methods

We divided this section into four parts. In the first part, we described a comprehensive dataset including the field observations of environmental conditions, leaf traits, and ΔT (made close to midday or midnight). In the second part, we built a trait-based leaf energy balance model and assessed the model's performance with field observations from the above dataset. In the third part, we performed a model sensitivity analysis to quantify to what extent leaf traits

mediate Δ*T* variability, and explore trait-Δ*T* relationships at the diel timescale. In the last part, we evaluated the model-derived trait-Δ*T* relationships by comparing them with field observations.

2.1 Data collection

2.1.1 Data collection close to midday

2.1.1.1 Study sites

We conducted field measurements at three forest sites: (1) a temperate mixed forest at the Mt. Changbai (CB, location: 42°24′N, 128°06′E) with a mean annual temperature (MAT) of 2.8^{o}C and mean annual precipitation (MAP) of 691 mm (He *et al*., 2019); (2) a tropical broadleaved evergreen forest at the Xishuangbanna site (XSBN, location: 21°47′N, 101°03′E) with a MAT of 21.8^{o}C and MAP of 1493 mm (Shen *et al*., 2018); and (3) a Caatinga woodland forest near Petrolina (PE, location: 9°03′S, 40°19′W), with a MAT of 26.2^{o}C and MAP of 510 mm (de Souza *et al*., 2018).

We selected these three sites for two reasons. First, we could access the sunlit leaves of representative canopy tree species of each site, which minimized other factors (e.g. illumination conditions) that also caused Δ*T* variability. Specifically, a canopy crane facility is available at each of the CB and XSBN sites that enabled easy access to canopy trees within a one-hectare area surrounding the canopy crane tower. At the PE site, we accessed sunlit canopy leaves using a horticultural ladder due to the relatively lower height of the trees (Majcher, 2018). Second, there was a vast diversity of biotic and abiotic conditions across these sites, including tree species, temperature, precipitation, and soil types (Cao *et al*., 2006; Wu *et al*., 2006), which allowed for a broader-scale evaluation of our model.

2.1.1.2 Field measurements of environmental variables, leaf traits, and ΔT

At the CB and XSBN sites, field measurements were conducted during the peak growing season (July-August) of 2019, and all the leaves surveyed were fully expanded leaves to minimize the effects of leaf age. Environmental variables including photosynthetically active radiation (PAR), air temperature (T_{air}), relative humidity (RH), and wind speed (u) were logged by a weather station (WatchDog 2550) at half-hour intervals. Four leaf traits: $V_{c,max25}$ (measured by portable gas exchange systems—LI-6400XT); visible and near-infrared light absorptance (α_{PAR} and α_{NIR}; measured by a spectrometer—Spectra Vista Corporation, SVC, HR-1024i); leaf width derived via the scanned images and ImageJ software (version 1.53); and T_{leaf} close to solar noon (measured by a thermal camera between 10:30 am and 1:30 pm, FLIR-T650sc AB, Band range: 7.5-13.0 μm) were measured for sunlit leaves from 19 canopy trees across 7 abundant tree species in CB and 26 canopy trees across 15 abundant tree species in XSBN (Table S1), following the protocols used in previous studies (Majcher, 2018; Wu *et al.*, 2019; Yan *et al.*, 2021).

At the PE site, field measurements were conducted during the middle-to-end of the growing season (February-May) of 2018 and all the leaves surveyed have been strictly controlled on the fully expanded leaves to minimize the effects of leaf age. The environmental variables collected (consistent with CB and XSBN sites) were derived from a local flux tower belonging to Embrapa Semi-Árido, Brazil. Leaf width, T_{leaf}, and ΔT close to solar noon were measured for sunlit leaves from 27 canopy trees across 13 most abundant Caatinga tree species (Table S1). It is worth noting that there were no measurements of leaf emissivity (ε_{leaf}) and g_1 in our three sites (Table 1).

2.1.2 Data collection close to midnight

At the CB, XSBN, and PE sites, we lacked night-time T_{leaf} and paired environmental observations to derive and validate the trait-ΔT relationship because the relevant facilities could not be used at night due to safety concerns. Thus, we turned to the datasets assembled from previous publications to retrieve environmental data, leaf traits, and ΔT. For this, in September 2021, we searched the Web of Science Core Collection database using the combined keywords of 'leaf temperature' and 'leaf traits' and 'night' as the search terms, returning a total of 204 peer-reviewed papers. We thoroughly reviewed these articles and checked whether they included paired night-time measurements of any of the six leaf traits in our model and all of the necessary environmental data to model T_{leaf}. Based on the above criteria, two papers, Lusk & Clearwater (2015) and Lusk *et al.* (2018), were found to include 90 leaves with paired measurements from 21 tree species of two temperate forest sites in New Zealand close to midnight.

From these papers, environmental variables, including air temperature, humidity, wind speed, and PAR (that was by default set zero at night), were recorded by meteorological sensors with data loggers. Leaf temperature was measured by a thermocouple. Only one trait, leaf width, was measured, and the other five traits in our model were not observed in any previous study.

2.2 Trait-based leaf energy balance model and model assessments

2.2.1 A trait-based leaf energy balance model

To represent trait-ΔT relationships in a mechanistic way, we built a trait-based model, in which leaf traits were used as model parameters. Our trait-based model integrated a plant physiology model (Wu *et al*., 2017) with a steady-state leaf energy balance model (Equations 1-2; Campbell & Norman, 2012), where leaf temperature (T_{leaf}; ^{o}C) or ΔT is derived based on

the balance between the net radiation flux (R_n; W m^{-2}), latent heat flux (λE; W m^{-2}), and sensible heat flux (H; W m^{-2}).

$$H = R_n - \lambda E \quad (1)$$

$$\Delta T = T_{\text{leaf}} - T_{\text{air}} = H/(c_p \times g_H) = (R_n - \lambda E)/(c_p \times g_H) \quad (2)$$

$$\lambda E = \lambda \times \frac{g_s \times g_b}{g_s + g_b} \times \text{VPD}_{leaf} \times \frac{1}{P_a} \quad (3)$$

where c_p refers to the specific heat capacity of air; g_s and g_b are stomatal conductance and boundary layer conductance for water vapour, respectively; P_a is the atmospheric pressure; g_H is boundary layer conductance and can be described as a function of leaf width (d) and wind speed (u) (see Table S2 for details). λE in Equation 3 is determined by the leaf-to-air VPD and diffusivity conductance (the function of g_s and g_b), where g_s can be described using a stomatal conductance model (Medlyn *et al.*, 2011). The Medlyn-type stomatal conductance model was used because it is a mechanistic model based on the optimality theory and has been shown to model g_s with high accuracy (e.g. Duursma, 2015; Wu *et al.*, 2020).

Because net assimilation rate (A_n), often characterized by the Farquhar-von Caemmerer-Berry photosynthesis model (FvCB; Farquhar *et al.*, 1980), is an essential input for the Medlyn-type g_s model, the coupling of the two models (FvCB-Medlyn model) would allow for direct modeling of g_s. The FvCB-Medlyn modeled g_s, together with leaf traits and environmental variables, is then used to derive the energy fluxes (e.g. λE) in the energy balance model (Janka *et al.*, 2016). Specifically, the integration of these models (i.e. leaf energy balance model and FvCB-Medlyn model) consists of three steps. First, the initial values of T_{leaf} (set as T_{air}) and C_i (set as 0.7×C_a, C_a=400 ppm), together with other relevant variables and parameters (e.g. $V_{\text{c,max}}$, PAR, and so on, see Table S4), were input into the FvCB model to obtain net photosynthesis rate (A_n) (indicated by the yellow box of Fig. S1). Second, after obtaining the A_n value, stomatal conductance (g_s) was then calculated using the Medlyn-type

model, followed with an update value on C_i based on the Equation of $C_i = C_a\text{-}1.6*A_n/g_s$ (Warren & Adams, 2006). We kept looping these two steps until the convergence of C_i and g_s (indicated by the green box in Fig. S1). Third, we input the g_s into the leaf energy balance equation to calculate the three energy fluxes (i.e. R_n, λE, and H) for deriving T_{leaf}, and kept looping all the above three steps until these energy fluxes being balanced (i.e. R_n -H- λE=0). As a result, the final modeled T_{leaf} was derived.

There are three types of model inputs in our trait-based leaf energy balance model. The first type includes six leaf traits (Fig. 1), namely, ε_{leaf}, α_{PAR}, α_{NIR}, d, $V_{c,max25}$, and g_1. We here did not include leaf mass per area (LMA, a key leaf trait in TBMs), since it is not directly linked to the leaf-level energy balance equation (see Fig. 1 and Equations in Table S2). The second type is environmental variables, including T_{air} (^{o}C), PAR (μmol m^{-2} s^{-1}), atmospheric CO_2 concentration (C_a; ppm), RH (%), and u (m s^{-1}). The third type is model constants, such as the specific heat capacity of air (c_p= 29.3 J mol^{-1} K^{-1}) and latent heat of vaporization of water (λ= 44000 J mol^{-1}). The details of these inputs are shown in Table S4.

Due to some higher-order nonlinear energy terms associated with T_{leaf} in the energy balance equations (e.g. Equations 4 & 18 of Table S2), there is no analytical solution for T_{leaf}. Instead, two alternative approaches are often proposed, namely, the linear approximation approach (Paw, 1987) and numerical solution (Gutschick, 2016). The linear approximation approach uses a linearized first/second-order Taylor approximation for the nonlinear terms, but its accuracy decreases with an increase in ΔT (Tracy *et al.*, 1984). In the second approach, the iteration process starts with assigning an initial value of T_{leaf} (e.g. T_{leaf}=T_{air}), followed by calculated intermediate variables and associated updated value of T_{leaf}, and then repeats the above process until the whole set of energy equations are balanced. In our study, we used the

second approach to solve T_{leaf} since it is more accurate (Gutschick, 2016). Our trait-based leaf energy balance model was coded in MATLAB (R2019a; MathWorks Inc., Natick, Massachusetts), following the framework and equations shown in Fig. S1 and Table S2-S3. Our code and all the data used in this study are available on this GitHub page: https://github.com/guozhengfei/trait-based-leaf-energy-balance-model.

2.2.2 Model assessments

To assess model accuracy, we compared modeled T_{leaf} and ΔT with corresponding field observations. Specifically, leaf traits and associated *in-situ* measurements of environmental variables at the CB and XSBN sites were used to drive the trait-based model (the details are shown in Table 1). As we didn't measure g_1 in our field records, we used a global synthesis study (Lin *et al.*, 2015) and assigned PFT (plant functional type)-specific g_1 values for CB (g_1=4.64) and XSBN (g_1=3.77), respectively. Our analysis shows strong agreements between both model-derived T_{leaf} and ΔT with field observations (Fig. S2; R^2=0.93 for T_{leaf} and R^2=0.71 for ΔT), consistent within and across the two forest sites.

2.3 Model sensitivity analysis

After model evaluation, we carried out a global sensitivity analysis on the trait-based model to address two questions: (1) To what extent do leaf traits regulate ΔT variability? (2) What are the most important traits that regulate ΔT variability, and how do their relative roles vary at the diel timescale? To address these two questions, we used a set of *in-situ* measurements of environmental variables as the model input while allowing the trait variability to cover the full range of values reported by the literature (Table 2).

There are four steps in the model sensitivity analysis. Step 1 is the set-up of environmental variables (Table 2). We used the *in-situ* diel measurements of all environmental variables (Fig. S3) except wind speed. The wind speed values were set as constants for daily averages following the similar protocol of Wright *et al*. (2017) to control the ΔT variability caused by the irregular disturbance of wind speed (Fig. S3d) while emphasizing the ΔT variability resulting strictly from the biotic controls. To further validate this approach, we conducted a series of model simulations, and demonstrated that despite the wind speed having a strong influence on the magnitude of ΔT (Fig. S4), the model-derived trait-ΔT relationships remained comparable across various wind speed scenarios (Fig. S5).

Step 2 is the set-up of leaf traits. We built up a one-time random sampling for each of all six leaf traits using Sobol' quasi-random sequences (Sobol' *et al*., 2011), each of which has a uniform distribution following a predefined trait range from the literature (Table 2). The uniform random sampling approach was used here based on an assumption that these six traits are independent of each other. To ensure this assumption is reasonable, we analyzed the correlations among four measured leaf traits (i.e. leaf size, PAR absorptance, NIR absorptance, and $V_{c,max25}$) and the result confirms no covariance among them (Fig. S6). We then performed an additional analysis with the sample size varying from 100 to 10000 and found that the explored trait-ΔT relationships stabilized when the sample size was above 2000 (Fig. S7). We thus used a sample size of 2000 for the construction of our random trait combinations.

Step 3 is model simulations using our trait-based leaf energy balance model. With the ensemble of trait combinations (n=2000) generated in step 2, together with the prescribed diel environmental variables (in half-an-hour intervals) in step 1, we ran the trait-based leaf

energy balance model to infer $T_{leaf}/\Delta T$, from which we further calculated the variability range of the modeled T_{leaf} and ΔT for each time step over the full diel timescale, addressing our question 1.

Step 4 is variance partitioning. For each time step (with constant environmental conditions) throughout the diel timescale, we employed a widely used global variance-based sensitivity analysis algorithm (EFAST, Saltelli *et al*., 2010), which captures both the direct and indirect effects of model parameters on model output. Using this method, we partitioned the variance of modeled T_{leaf} and ΔT to the variability of each leaf trait, addressing our question 2.

We also output several intermediate model state variables, including R_n, λE, and g_H, to help explain the mechanism underlying traits' role in regulating ΔT variability at the diel timescale.

2.4 Trait-ΔT relationships evaluation with field observations

To address our question 3 (Do modeled trait-ΔT relationships agree with field observations?), we evaluated model-derived trait-ΔT relationships against field observations made close to midday or midnight (Table 3). Here, traits' relative importance on ΔT could be represented by the R^2 of trait-ΔT, the higher the corresponding R^2, the greater the relative importance,(Fig. S8). For the midday evaluation, we used field measurements made close to local solar noon (10:30 am-1:30 pm) under clear-sky days at our three forest sites, and analysed the relationships of ΔT with $V_{c,max25}$, α_{PAR}, α_{NIR}, and leaf width. For the midnight evaluation, we used field observations (made close to midnight around between 0:00 am and 2:00 am) assembled from previous publications (i.e. Lusk & Clearwater, 2015; Lusk *et al.*, 2018), including leaf width, ΔT, and relevant environmental data, to derive and evaluate the leaf trait-ΔT relationship. Regardless of the trait-ΔT relationships derived from models and

observations, we used ordinary least-squares regressions to examine these relationships. It is also important to note that the trait-based energy balance model was driven by the same set of environmental variables corresponding to field-based paired measurements of traits and ΔT for each site (Table 3).

3. Results

3.1 Diel variations in model-derived T_{leaf} and ΔT

The diel patterns were assessed with two metrics, the mean and range of T_{leaf} and ΔT, both of which showed large but consistent diel patterns across all the three forest sites (Fig. 2). Specifically, for each site, we observed that both environmental variables and leaf traits drove the diel variations in T_{leaf} and ΔT, with the diel changes in mean T_{leaf} and ΔT primarily driven by the diel environmental variability since the same set of leaf traits were used throughout the day. However, as the environmental conditions were set constant for each half-hour time point, the range of T_{leaf} and ΔT (i.e. the error bars in Fig. 2) was caused solely by leaf traits.

The diurnal variation in ΔT could further be divided into the following three phases: 1) from early morning to middle afternoon (e.g. 6 am to 4 pm in Fig. 2a-ii), ΔT was positive with an initial increase in its mean and range until peak (*c.* 15.0°C in ΔT range) at noon, followed with slight declines afterwards; 2) from mid-afternoon to sunset (e.g. 4 pm to 8 pm in Fig. 2a-ii), ΔT was all negative with continuous decreases in its mean and range; and 3) during the night-time (e.g. before 6 am or after 8 pm in Fig. 2a-ii), ΔT was all negative and nearly constant for both its mean (*c.* -2.0°C) and range (*c.* 3.0°C).

To explore the drivers of the diel ΔT variation, we assessed the diel dynamics of R_n, λE, and g_H that determined ΔT. We observed nearly constant mean and range values of g_H across the

full diel timescale (Fig. 2a,b,c-iii), suggesting that g_H was not the state variable responsible for the model-derived ΔT variability. In contrast, R_n and λE demonstrated significant diurnal variations, and the difference between these two variables (R_n-λE) precisely tracked the diurnal pattern in ΔT in terms of both sign and range of its variability, with positive R_n-λE leading to positive ΔT and *vice versa* (Fig. 2a,b,c-iv). For night-time, since λE=0, the ΔT variability was primarily determined by the ratio of R_n/g_H, where R_n and g_H were both nearly constant in their means and ranges (Fig. 2a,b,c-iii and Fig. 2a,b,c-iv), resulting in relatively stable ΔT during the night-time (Fig. 2a,b,c-ii).

3.2 Relative importance of leaf traits in regulating ΔT variability at the diel timescale

Our results identified leaf width, $V_{c,max25}$, and g_1 as the three most important traits that cumulatively explained over 90% of ΔT variability. Their relative importance was not static, showing strong variations across the full diel timescale (Fig. 3). During night-time, leaf width explained over 90% of the model-derived ΔT variability, with leaf emissivity accounting for the remaining part. During day-time, g_1 and $V_{c,max25}$ had increased relative importance, and together with leaf width explained around 90% of the ΔT variability (Figs. 3 and S10). Specifically, the relative importance of these three traits was observed to follow a W-shaped pattern during day-time, and the timing when T_{leaf} equals T_{air} because $R_n = \lambda E$ determined the critical transition points of the W-shape, during which the relative role of leaf width was diminished while showing a higher value before and afterwards. In contrast, the relative importance of g_1 and $V_{c,max25}$ showed complementary and inversed trends to that of leaf width. Finally, we demonstrated a varying response of each state variable (i.e. R_n, g_H, and λE) to specific leaf traits as the main reason for why traits displayed varied importance in regulating ΔT (Fig. 4).

3.3 Evaluations of the model-derived trait-Δ*T* relationships with field observations

For midnight, only one trait, leaf width, was found to have been reported in the literature matching our search criteria. Regardless, both field observations and model results demonstrated that leaf width explained most of the night-time Δ*T* variability, with Δ*T* decreasing exponentially with leaf width (R^2=0.89 for observations and R^2=0.97 for model; Fig. 5), agreeing with other studies (Wright *et al*., 2017; Lusk *et al*., 2018). During midday, among the four traits analysed ($V_{c,max25}$, leaf width, α_{PAR}, and α_{NIR}), the trait-Δ*T* relationships derived from field observations and model were very comparable (Fig. 6). Specifically, both observations and model demonstrated a negative exponential relationship between $V_{c,max25}$ and Δ*T* (R^2=0.17-0.33 for observations and R^2=0.22 for model; Fig. 6a), a positive exponential relationship between leaf width and Δ*T* (Fig. 6b), and weak relationships between Δ*T* with α_{PAR} and α_{NIR} (Fig. 6c-d).

4. Discussion

4.1 Important biotic regulations of Δ*T* variability

For long, plant species have been suggested to be characterized by a set of plant traits (Wright *et al*., 2004; Weng *et al*., 2017; Franklin *et al.*, 2020). Here, we used a trait-based leaf energy balance model to investigate the dominant biotic controls on Δ*T*. Our results demonstrate that the range of Δ*T* variability is strongly mediated by a combination of leaf traits (Fig. 2a,b,c-ii) across the diel timescale. The observed large variability in trait-mediated Δ*T*, including the range of Δ*T* variability peak at noon (from -2.9 to 11.9℃) and minimum at midnight (from -3.5 to -0.1℃), is consistent with several previous field-based studies. For example, researchers found that the Δ*T* variation at the interspecific level varied from 0.3 to 4.8℃ in a mixed temperate deciduous forest in Switzerland (Leuzinger & Körner, 2007), and -2.8 to 7.5℃ in a tropical evergreen forest in Southeast China (Dong *et al*., 2016). Meanwhile,

consistently negative night-time ΔT across species ranging from -3.2 to -0.8℃ in a temperate deciduous forest in New Zealand (Lusk *et al*., 2018) and from -3.0 to -0.5℃ in a desert plant community in Egypt (Hegazy & El Amry, 1998) were also observed. Our results, together with these previous studies, highlight the importance of leaf traits in regulating ΔT variability.

Our finding of large trait-associated ΔT variability also calls for caution on using ΔT for plant health monitoring (Gerhards *et al*., 2016; Jin *et al*., 2017). Recently, the monitoring of T_{leaf} or ΔT has been increasingly advocated as an integral component for plant health monitoring, since under similar environmental conditions, a higher T_{leaf} or ΔT is more likely associated with reduced plant transpiration and water stress statuses (Isoda, 2010; Gerhards *et al*., 2016; Niu & Xiang, 2018). This approach might work well when tracking the same plant species across local-space and limited-time scales (Jones & Leinonen, 2003; Sagan *et al*., 2019). However, it is risky when monitoring species-rich vegetative communities where trait-induced ΔT variability can be large, as a higher ΔT may be caused exclusively by leaf traits rather than stress status (e.g. Fig. 2). Consequently, we recommend considering these intrinsic biotic regulations of ΔT when using thermal remote sensing techniques to monitor plant health statuses.

4.2 Dynamic relative importance of leaf traits in regulating ΔT variability at the diel timescale

Our study demonstrated that leaf width, $V_{c,max25}$, and g_1 are the three dominant traits regulating ΔT, followed by α_{NIR}, α_{PAR}, and emissivity (Fig. 3). Although leaf width regulating ΔT through altering leaves' boundary larger conductance has been well known (Jones, 2013; Aubrecht *et al*., 2016), the dominant role of g_1 and $V_{c,max25}$ on ΔT regulation has rarely been reported previously. g_1 and $V_{c,max25}$ regulate T_{leaf} and ΔT primarily because they control the

456 stomatal behaviours, and thus cooling air temperature through leaf transpiration. Specifically,
457 as shown in Equation 4 (Medlyn *et al*., 2011), under a given environmental condition, g_s
458 scales linearly with stomatal slope (g_1) and net assimilation rate (A_n), which is positively
459 correlated with $V_{c,max25}$ (Farquhar *et al*., 1980).

460 $$g_s = 1.6 \times \left(1 + \frac{g_1}{\sqrt{VPD}}\right) \times \frac{A_n}{C_a},\ A_n \propto V_{c,max25} \quad (4)$$

461

462 Additionally, the relative importance of leaf traits in regulating ΔT is not static, instead, they
463 show strong diel variation (Fig. 3). To our knowledge, this is the first study uncovering a
464 novel insight into diel changes in the proportionate importance of leaf traits in regulating ΔT
465 dynamics. Meanwhile, the dynamic traits-ΔT relationship derived by our trait-based model
466 during night-time and day-time is further confirmed with field observations (Figs. 4 and 5).
467 These dynamic trait-ΔT relationships further suggest that previous empirical explorations of
468 trait-ΔT relationships that focus on either some traits with no direct links with leaf energy
469 balance (e.g. leaf circularity; Majcher, 2018) or certain fixed time point of measurements (e.g.
470 Leuzinger & Körner, 2007; Leigh *et al*., 2012) are limited. A recent study has also pointed
471 out that traits that are common but not directly linked to energy balance (e.g. nitrogen
472 fraction and $\delta^{13}C$) are not very useful in predicting T_{leaf} or ΔT (Blonder *et al*., 2020).

473

474 The reason for the change in the relative importance of leaf traits in regulating ΔT is that R_n,
475 H, and λE jointly determine ΔT, while each of them is jointly determined by both
476 environmental variables (change throughout the day) and associated leaf traits (Fig. 1). For
477 example, as shown in Fig. 2, R_n displays a clear diel trend following a similar shape as the
478 diel pattern of PAR. Diurnal variation in λE is tightly related to diurnal variation in leaf
479 ecophysiology (i.e. stomatal conductance tied to $V_{c,max25}$ and g_1) and VPD (Figs 2 and S4).
480 Since the diurnal patterns in R_n and λE are different, it further suggests that the relative roles

of R_n and λE in determining ΔT (proportional to R_n-λE) can be different across the diel time scale. Together with the different roles of each trait on mediating R_n and λE (Fig. 4), these ultimately lead to the dynamic relative role of each trait in regulating ΔT.

With these findings, our work generates two implications. Firstly, our observed diel variation in leaf width-ΔT relationships helps explain the macro patterns of leaf width distribution across large environmental gradients. Consistent with several previous field-based studies (Lusk *et al*., 2018; Majcher, 2018), our results demonstrate a tight and negative leaf width-ΔT relationship during night-time (Fig. 5) and a positive leaf width-ΔT relationship during day-time (Fig. 6b). The observed negative leaf width-ΔT relationship at night may imply that plants living in cold regions tend to maintain smaller leaf width to avoid night-time over-cooling. The observed positive leaf width-ΔT relationship during day-time may imply that plants living in hot and dry environments tend to maintain smaller leaf width to avoid day-time overheating. Both of them are consistent with many empirical observations that have been conducted across large temperature (Peppe *et al*., 2011; Wright *et al*., 2017; Lusk *et al*., 2018) or rainfall (McDonald *et al*., 2003; Li *et al*., 2020) gradients. These together suggest that trait-mediated plant thermoregulation can be an important strategy to help interpret macroecological patterns of climate-trait relationships, and our trait-based leaf energy balance model could be a potential tool for this exploration. In addition to leaf thermoregulation as a candidate strategy, it is also worth noting that many other factors (e.g. plant height, water, light, and nutrient availability) can operate as alternative mechanisms in structuring the biogeography of leaf width (Wright *et al*., 2017; Lusk *et al*., 2018).

Secondly, both our modeled and field-derived trait-ΔT relationships highlight that there are key leaf traits regulating ΔT and should be accurately represented in modeling. Since the

overall framework of our trait-based modeling approach is similar to that module in TBMs, our findings have direct implications for TBMs as well. The leaf energy balance model has long been a critical component for simulating plant ecophysiological responses in TBMs (Oleson *et al.*, 2010; Lawrence *et al.*, 2018), but their trait parameterization remains oversimplified, e.g. assigning fixed trait values for each plant functional type, resulting in the large modeling uncertainty (Rogers *et al.*, 2017; Fisher *et al.*, 2018). Our finding of large modeled trait-mediated ΔT variability, as well as the dynamics of traits' relative roles throughout the diel timescale, suggests the importance of incorporating multiple traits, particularly leaf width, $V_{c,max25}$, and g_1, and associated trait variability in TBMs.

4.3 Caveats and future directions

Our work also has two important caveats that need to be improved in the future. First, our demonstration of biotic regulations of ΔT relied on a specific abiotic condition (i.e. clear-sky days and without environmental stress). This simplification was essential to help understand the dominant biotic controls, but is not complete as ΔT is jointly determined by leaf traits and environmental conditions (see our trait-based leaf energy balance model and also Michaletz *et al.*, 2015; Gutschick, 2016). Especially when plants are under environmental stress, e.g. extreme heat/drought environment, leaves may have a thermal response that differs from normal conditions, because atmospheric water demand (VPD) increases but soil water supply (e.g. soil moisture) decreases, affecting the plant water use efficiency (reflected by the change in leaf water potential, g_1 and $V_{c,max25}$; e.g. Zhou *et al.*, 2014; Anderregg *et al.*, 2017), transpiration, and thus T_{leaf}. Additionally, we only collected paired measurements of ΔT and leaf traits at the peak growing season of limited sites close to midday or midnight to validate our results, with a lack of observations at other time points throughout the diel timescale or other seasons of the year. Therefore, a comprehensive understanding and model evaluation of

the ΔT variability across more representative field sites over various environmental conditions (e.g. across the full growing season or under environmental stress) and the full diel timescale is still needed.

Second, to minimize additional sources of uncertainty, we focused this study on the leaf level and did not consider night-time transpiration. However, night-time transpiration for some plants cannot be ignored (Caird *et al*., 2007*;* Sadok & Jagadish, 2020), and should be considered in future studies. Meanwhile, the understanding of dominant biotic regulations of ΔT at the canopy or ecosystem level is even more important, but is more challenging as well (Gutschick, 2016; Zellweger *et al*., 2019). Larger scales representing entire plants or forest ecosystems as a whole responding to the ambient environment can be evaluated with measurements of sap flow, eddy covariance, and proximate and satellite remote sensing (Doughty *et al*., 2008; Newman *et al*., 2019). With the validation of the trait-based energy balance model in this study, the next important step is to extend the current modeling work from leaf to canopy and ecosystem levels, which ultimately allows us to quantitatively assess the roles of canopy structure, leaf traits, and microclimate (Jucker *et al*., 2018; Zellweger *et al*., 2019) in regulating ΔT variability from individual plants to forest ecosystems. The global plant traits dataset (e.g. TRY; Kattge *et al*., 2020) and the technique using vegetation spectroscopy to infer leaf traits (Serbin *et al*., 2015; Wu *et al*., 2019) would offer important datasets for such scaling exploration, and these efforts are still greatly needed in the future.

5. Conclusions

In this study, we developed a coupled trait-based leaf energy balance model to explore the role of different leaf traits in mediating leaf thermoregulation (approximated by ΔT). Our results show that leaf traits were important regulators of ΔT variability across the full diel

timescale (Fig. 2), highlighting the importance of considering biotic controls when predicting leaf temperature. Among the six leaf traits included in the model, leaf width, $V_{c,max25}$, and g_1 were the most important, and their relative importance in regulating ΔT varied considerably throughout the day (Fig. 3), agreeing with field observations (Figs. 5 and 6). This suggests these three are the key leaf traits that need to be accurately parameterized when modeling leaf temperature and associated physiological processes, as well as in TBMs aiming to study the large-scale pattern of vegetation and atmosphere interactions. Collectively, our study improves the process understanding of biotic regulations of ΔT, offering a trait-based mechanistic approach to improve our understanding of leaf thermoregulation strategies across plant individuals and associated modeling of plant physiological response to climate variability.

Acknowledgments

This work was supported by National Natural Science Foundation of China (# 31922090), Hong Kong Research Grants Council Early Career Scheme (#27306020). J.W. was in part supported by the Innovation and Technology Fund (funding support to State Key Laboratories in Hong Kong of Agrobiotechnology) of the HKSAR, China. C.K.F. Lee was in part supported by HKU seed fund for basic research (#202011159154) and the HKU 45th round PDF scheme. H.-M.L. was supported by the Hong Kong Research Grants Council Area of Excellence Scheme (AOE/M-403/16). M. W. thanks the funding support from a grant by the General Research Fund (Grant no. 15603920), and the Research Institute for Sustainable Urban Development (Grant no. 1-BBWD), the Hong Kong Polytechnic University. The authors would like to thank Mr. Guanhua Dai and Mr. Jinlong Dong for canopy crane access assistance and acknowledge the support of the National Forest Ecosystem Research Station at Xishuangbanna for providing *in-situ* measurements of meteorological data. We would also like to thank Dr. Magna Soelma Beserra de Moura for providing us with the meteorological measurements from the flux tower of Embrapa Semiárido near Petrolina, Pernambuco, and thank Dr. Ensheng Weng for many very insightful comments on the early version of this manuscript.

Author contributions

J.W. and Z.G. designed the study. Z.G., Z.Y., B.M.M., Y.Z., G.S., B.W., X.W., Y.D., and J.W. contributed to data collection. Z.G. and J.W. carried out all the data analyses, and Z.Y., B.M.M., C.K.F.L., S.T.M., Y.R., A.L., H.-M.L., M.W., and L.L. participated in the result interpretation. Z.G, Y.Z., B.M.M., C.K.F.L., and J.W. drafted the paper and all authors contributed to the writing of the manuscript.

References

Anderegg WR, Wolf A, Arango-Velez A, Choat B, Chmura DJ, Jansen S, Kolb T, Li S, Meinzer F, Pita P, Resco de Dios V. 2017. Plant water potential improves prediction of empirical stomatal models. *PloS one*. **12**:e0185481.

Aubrecht DM, Helliker BR, Goulden ML, Roberts DA, Still CJ, & Richardson AD. 2016. Continuous, long-term, high-frequency thermal imaging of vegetation: Uncertainties and recommended best practices. *Agricultural and Forest Meteorology* **228**: 315-326.

Bernacchi CJ, Bagley JE, Serbin SP, RUIZ‐VERA UM, Rosenthal DM, & Vanloocke A. 2013. Modeling C3 photosynthesis from the chloroplast to the ecosystem. *Plant, Cell & Environment* **36:** 1641-1657.

Best MJ, Pryor M, Clark DB, Rooney GG, Essery R, Ménard CB, Edwards JM, Hendry MA, Porson A, Gedney N et al. 2011. The Joint UK Land Environment Simulator (JULES), model description–Part 1: energy and water fluxes. *Geoscientific Model Development* **4**: 677-99.

Bonan GB, Doney SC. 2018. Climate, ecosystems, and planetary futures: The challenge to predict life in Earth system models. *Science*. doi:10.1126/science.aam8328

Bonan GB, Williams M, Fisher R A, & Oleson K W. 2014. Modeling stomatal conductance in the earth system: linking leaf water-use efficiency and water transport along the soil-plant-atmosphere continuum. *Geoscientific Model Development* **7**: 2193-2222.

Campbell GS, Norman J. 2012. *An introduction to environmental biophysics*: Springer Science & Business Media.

Cao M, Zou X, Warren M, & Zhu H. 2006. Tropical forests of xishuangbanna, China[1]. *Biotropica: The Journal of Biology and Conservation* **38**: 306-309.

Chen C. 2015. Determining the leaf emissivity of three crops by infrared thermometry. *Sensors* **15**: 11387-11401.

de Souza LSB, de Moura MSB, Sediyama GC, da Silva TGF. 2018. Carbon exchange in a caatinga area during an unusually drought year. *Agrometeoros* **25**: 37-45.

Derroire G, Powers JS, Hulshof CM, Varela LEC, Healey JR. 2018. Contrasting patterns of leaf trait variation among and within species during tropical dry forest succession in Costa Rica. *Scientific Reports* **8**: 285.

Økland RH. 2007. Wise use of statistical tools in ecological field studies. *Folia Geobotanica* **42**:123-40.

Dong N, Prentice IC, Harrison SP, Song QH, Zhang YP. 2017. Biophysical homoeostasis of leaf temperature: A neglected process for vegetation and land-surface modeling. *Global Ecology and Biogeography* **26**: 998-1007.

Duursma, RA. 2015. Plantecophys - An R Package for Analysing and Modeling Leaf Gas Exchange Data. *PloS one*. doi:10.1371/journal.pone.0143346

Duursma, RA, Medlyn BE. 2012. MAESPA: a model to study interactions between water limitation, environmental drivers and vegetation function at tree and stand levels, with an example application to [CO_2]× drought interactions. *Geoscientific Model Development Discussions* **5**: 919–940.

Farquhar GD, von Caemmerer Sv, Berry JA. 1980. A biochemical model of photosynthetic CO2 assimilation in leaves of C 3 species. *Planta* **149**: 78-90.

Fauset S, Freitas HC, Galbraith DR, Sullivan MJP, Aidar MPM, Joly CA, Phillips OL, Vieira SA, Gloor MU. 2018. Differences in leaf thermoregulation and water use strategies between three co-occurring Atlantic forest tree species. *Plant Cell Environ* **41**: 1618-1631.

Féret JB, Gitelson A, Noble S, Jacquemoud S. 2017. PROSPECT-D: Towards modeling leaf optical properties through a complete lifecycle. *Remote Sensing of Environment* **193**: 204-215.

Fisher RA, Koven CD, Anderegg WR, Christoffersen BO, Dietze MC, Farrior CE, Holm JA, Hurtt GC, Knox RG, Lawrence PJ et al. 2018. Vegetation demographics in Earth System Models: A review of progress and priorities. *Global Change Biology* **24**: 35-54.

Franklin O, Harrison SP, Dewar R, Farrior CE, Brännström Å, Dieckmann U, Pietsch S, Falster D, Cramer W, Loreau M et al. 2020. Organizing principles for vegetation dynamics. *Nature Plants* **6**: 1-10.

Gates DM. 1968. Transpiration and leaf temperature. *Annual Review of Plant Physiology* **19**: 211-238.

Gerhards M, Rock G, Schlerf M, Udelhoven T. 2016. Water stress detection in potato plants using leaf temperature, emissivity, and reflectance. *International Journal of Applied Earth Bbservation and Geoinformation* **53**: 27-39.

Gutschick VP. 2016. Leaf Energy Balance: Basics, and Modeling from Leaves to Canopies. In *Canopy Photosynthesis: From Basics to Applications* (pp. 23-58).

He N, Liu C, Piao S, Sack L, Xu L, Luo Y, He J, Han X, Zhou G, Zhou X et al. 2019. Ecosystem traits linking functional traits to macroecology. *Trends in Ecology & Evolution* **34**: 200-210.

Hegazy A, El Amry M. 1998. Leaf temperature of desert sand dune plants: perspectives on the adaptability of leaf morphology. *African Journal of Ecology* **36**: 34-43.

Helliker BR, Richter SL. 2008. Subtropical to boreal convergence of tree-leaf temperatures. *Nature* **454**: 511-514.

Huang CW, Chu CR, Hsieh CI, Palmroth S, Katul GG. 2015. Wind-induced leaf transpiration. *Advances in Water Resources* **86**: 240-255.

Huang M, Piao S, Ciais P, Peñuelas J, Wang X, Keenan TF, Peng S, Berry JA, Wang K, Mao J et al. 2019. Air temperature optima of vegetation productivity across global biomes. *Nature Ecology & Evolution* **3**: 772-779.

Isoda A. 2010. Effects of water stress on leaf temperature and chlorophyll fluorescence parameters in cotton and peanut. *Plant Production Science* **13**: 269-278.

Ivanova LA, Zolotareva NV, Ronzhina DA, Podgaevskaya EN, Migalina SV, Ivanov LA. 2018. Leaf functional traits of abundant species predict productivity in three temperate herbaceous communities along an environmental gradient. *Flora* **239**: 11-19.

Janka E, Körner O, Rosenqvist E, Ottosen CO. 2016. A coupled model of leaf photosynthesis, stomatal conductance, and leaf energy balance for chrysanthemum (Dendranthema grandiflora). *Computers and Electronics in Agriculture* **123**: 264-274.

Jin M, Liu X, Zhang B. 2017. Evaluating heavy-metal stress levels in rice using a theoretical model of canopy-air temperature and leaf area index based on remote sensing. *IEEE Journal of Selected Topics in Applied Earth Observations and Remote Sensing* **10**: 3232-3242.

Jones HG. 1999. Use of thermography for quantitative studies of spatial and temporal variation of stomatal conductance over leaf surfaces. *Plant, Cell & Environment* **22**: 1043-1055.

Jones HG. 2013. *Plants and microclimate: a quantitative approach to environmental plant physiology*. Cambridge university press.

Jones HG, Leinonen I. 2003. Thermal imaging for the study of plant water relations. *Journal of Agricultural Meteorology* **59**: 205-217.

Jucker T, Hardwick SR, Both S, Elias DM, Ewers RM, Milodowski DT, Swinfield T, Coomes DA. 2018. Canopy structure and topography jointly constrain the microclimate of human‐modified tropical landscapes. *Global Change Biology* **24**: 5243-5258.

Kattge J, Bönisch G, Díaz S, Lavorel S, Prentice IC, Leadley P, Tautenhahn S, Werner GD, Aakala T, Abedi M et al. 2020. TRY plant trait database–enhanced coverage and open access. *Global Change Biology* **26**: 119-188.

Lawrence D, Fisher R, Koven C, Oleson K, Swenson S, Vertenstein M, Andre B, Bonan G, Ghimire B, van Kampenhout L et al. 2018. Technical description of version 5.0 of the Community Land Model (CLM). *National Center for Atmospheric Research, University Corporation for Atmospheric Research, Boulder, CO*.

Leigh A, Sevanto S, Ball MC, Close JD, Ellsworth DS, Knight CA, Nicotra AB, Vogel S. 2012. Do thick leaves avoid thermal damage in critically low wind speeds? *New Phytologist* **194**: 477-487.

Leigh A, Sevanto S, Close J, Nicotra A. 2017. The influence of leaf size and shape on leaf thermal dynamics: does theory hold up under natural conditions? *Plant, Cell & Environment* **40**, 237-248.

Leuzinger S, Körner C. 2007. Tree species diversity affects canopy leaf temperatures in a mature temperate forest. *Agricultural and Forest Meteorology* **146**: 29-37.

Leuzinger S, Vogt R, Körner C. 2010. Tree surface temperature in an urban environment. *Agricultural and Forest Meteorology* **150**: 56-62.

Li Y, Zou D, Shrestha N, Xu X, Wang Q, Jia W, Wang Z. 2020. Spatiotemporal variation in leaf size and shape in response to climate. *Journal of Plant Ecology* **13**:87-96.

Lin YS, Medlyn BE, Duursma RA, Prentice IC, Wang H, Baig S, Eamus D, De Dios VR, Mitchell P, Ellsworth DS et al. 2015. Optimal stomatal behaviour around the world. *Nature Climate Change* **5**: 459-464.

Lloyd J, Farquhar GD. 2008. Effects of rising temperatures and [CO2] on the physiology of tropical forest trees. *Philosophical Transactions of the Royal Society B: Biological Sciences* **363**: 1811-1817.

Lusk CH, Clearwater MJ. 2015. Leaf temperatures of divaricate and broadleaved tree species during a frost in a North Island lowland forest remnant, New Zealand. *New Zealand Journal of Botany* **53**: 202-209.

Lusk CH, Clearwater MJ, Laughlin DC, Harrison SP, Prentice IC, Nordenstahl M, Smith B. 2018. Frost and leaf-size gradients in forests: global patterns and experimental evidence. *New Phytolpgist **219*** : 565-573.

Majcher BM. 2018. *Leaf thermoregulation in the semi-arid tropics of Brazil.* Master thesis, Imperial College London.

McDonald P, Fonseca C, McC J, Westoby M. 2003. Leaf-size divergence along rainfall and soil-nutrient gradients: is the method of size reduction common among clades? *Functional Ecology* **1**: 50-57.

Medlyn BE, Duursma RA, Eamus D, Ellsworth DS, Prentice IC, Barton CV, Crous KY, De Angelis P, Freeman M, Wingate L. 2011. Reconciling the optimal and empirical approaches to modeling stomatal conductance. *Global Change Biology* **18**: 3476-3476.

Michaletz ST, Weiser MD, Zhou JZ, Kaspari M, Helliker BR, Enquist BJ. 2015. Plant Thermoregulation: Energetics, Trait-Environment Interactions, and Carbon Economics. *Trends in Ecology & Evolution* **30**: 714-724.

Murray FW. 1967. On the computation of saturation vapor pressure. *Journal of Applied Meteorology and Climateology* **6**: 203-204.

Newman EA, Kennedy MC, Falk DA, McKenzie D. 2019. Scaling and complexity in landscape ecology. *Frontiers in Ecology and Evolution* **7**: 293.

Niu Y, Xiang Y. 2018. An overview of biomembrane functions in plant responses to high-temperature stress. *Frontiers in Plant Science* **9**: 915.

Oleson KW, Lawrence DM, Bonan GB, Drewniak B, Huang M, Koven CD, Levis S, Li F, Riley W, Subin Z et al. 2010. Technical description of version 4.5 of the Community Land Model (CLM), NCAR Tech. *Notes (NCAR/TN-478+ STR)*.

Paw U KT. 1987. Mathematical analysis of the operative temperature and energy budget. *Journal of Thermal Biology* **12**: 227-233.

Peppe DJ, Royer DL, Cariglino B, Oliver SY, Newman S, Leight E, Enikolopov G, Fernandez‐Burgos M, Herrera F, Adams JM, Correa E. 2011. Sensitivity of leaf size and shape to climate: global patterns and paleoclimatic applications. *New Phytologist* **190**: 724-739.

Rogers A. 2014. The use and misuse of Vc,max in Earth System Models. *Photosynthesis Research* **119**: 15-29.

Rogers A, Serbin SP, Ely KS, Sloan VL, Wullschleger SD. 2017. Terrestrial biosphere models underestimate photosynthetic capacity and CO_2 assimilation in the Arctic. *New Phytologist* **216**: 1090-1103.

Sagan V, Maimaitijiang M, Sidike P, Eblimit K, Peterson KT, Hartling S, Esposito F, Khanal K, Newcomb M, Pauli D. 2019. UAV-based high resolution thermal imaging for vegetation monitoring, and plant phenotyping using ICI 8640 P, FLIR Vue Pro R 640, and thermomap cameras. *Remote Sensing* **11**: 330.

Saltelli A, Annoni P, Azzini I, Campolongo F, Ratto M, Tarantola S. 2010. Variance based sensitivity analysis of model output. Design and estimator for the total sensitivity index. *Computer Physics Communications* **181**: 259-270.

765 **Serbin SP, Singh A, Desai AR, Dubois SG, Jablonski AD, Kingdon CC, Kruger EL,**
766 **Townsend PA. 2015.** Remotely estimating photosynthetic capacity, and its response
767 to temperature, in vegetation canopies using imaging spectroscopy. *Remote Sensing of*
768 *Environment* **167**: 78-87.
769 **Shen T, Corlett RT, Song L, Ma WZ, Guo XL, Song Y, Wu Y. 2018.** Vertical gradient in
770 bryophyte diversity and species composition in tropical and subtropical forests in
771 Yunnan, SW China. *Journal of Vegetation Science* **29**: 1075-1087.
772 **Smith MN, Taylor TC, van Haren J, Rosolem R, Restrepo-Coupe N, Adams J, Wu J, de**
773 **Oliveira RC, da Silva R, de Araujo AC et al. 2020.** Empirical evidence for
774 resilience of tropical forest photosynthesis in a warmer world. *Nature Plants* **6**: 1225-
775 1230.
776 **Sobol' IM, Asotsky D, Kreinin A, Kucherenko S. 2011.** Construction and comparison of
777 high‐dimensional Sobol'generators. *Wilmott* **201**: 64-79.
778 **Song Q, Sun C, Deng Y, Bai H, Zhang Y, Yu H, Zhang J, Sha L, Zhou W, Liu Y. 2020.**
779 Tree Surface Temperature in a Primary Tropical Rain Forest. *Atmosphere* **11**: 798.
780 **Still C, Powell R, Aubrecht D, Kim Y, Helliker B, Roberts D, Richardson AD, Goulden**
781 **M. 2019.** Thermal imaging in plant and ecosystem ecology: applications and
782 challenges. *Ecosphere.* doi.org/10.1002/ecs2.2768.
783 **Still CJ, Rastogi B, Page GF, Griffith DM, Sibley A, Schulze M, Hawkins L, Pau S,**
784 **Detto M, Helliker BR. 2021.** Imaging canopy temperature: shedding (thermal) light
785 on ecosystem processes. *New Phytologist* **230:** 1746–1753.
786 **Tracy CR, van Berkum FH, Tsuji JS, Stevenson R, Nelson JA, Barnes BM, Huey RB.**
787 **1984.** Errors resulting from linear approximations in energy balance equations.
788 *Journal of Thermal Biology* **9**: 261-264.

Weng E, Farrior CE, Dybzinski R, Pacala SW. 2017. Predicting vegetation type through physiological and environmental interactions with leaf traits: evergreen and deciduous forests in an earth system modeling framework. *Global Change Biology* **23**: 2482-2498.

Wright IJ, Dong N, Maire V, Prentice IC, Westoby M, Díaz S, Gallagher RV, Jacobs BF, Kooyman R, Law EA et al. 2017. Global climatic drivers of leaf size. *Science* **357**: 917-921.

Wright IJ, Reich PB, Westoby M, Ackerly DD, Baruch Z, Bongers F, Cavender-Bares J, Chapin T, Cornelissen JH, Diemer M, F et al. 2004. The worldwide leaf economics spectrum. *Nature* **428**: 821-827.

Wright WE, Leavitt SW. 2006. Boundary layer humidity reconstruction for a semiarid location from tree ring cellulose δ18O. *Journal of Geophysical Research: Atmospheres* **111**: D18105.

Wu J, Albert LP, Lopes AP, Restrepo-Coupe N, Hayek M, Wiedemann KT, Guan K, Stark SC, Christoffersen B, Prohaska N et al. 2016. Leaf development and demography explain photosynthetic seasonality in Amazon evergreen forests. *Science* **351**: 972-976.

Wu J, Guan D, Sun X, Zhang M, Shi T, Han S, Jin C. 2006. Photosynthetic characteristics of dominant tree species and canopy in the broadleaved Korean pine forest of Changbai Mountains. *Science in China Series D: Earth Sciences* **49**: 89-98.

Wu J, Guan K, Hayek M, Restrepo‐Coupe N, Wiedemann KT, Xu X, Wehr R, Christoffersen BO, Miao G, da Silva R et al. 2017. Partitioning controls on Amazon forest photosynthesis between environmental and biotic factors at hourly to interannual timescales. *Global Change Biology* **23**: 1240-1257.

Wu J, Rogers A, Albert LP, Ely K, Prohaska N, Wolfe BT, Oliveira Jr RC, Saleska SR, Serbin SP. 2019. Leaf reflectance spectroscopy captures variation in carboxylation capacity across species, canopy environment and leaf age in lowland moist tropical forests. *New Phytologist* **224**: 663-674.

Wu J, Serbin SP, Ely KS, Wolfe BT, Dickman LT, Grossiord C, Michaletz ST, Collins AD, Detto M, McDowell NG et al. 2020. The response of stomatal conductance to seasonal drought in tropical forests. *Glob Chang Biology* **26**: 823-839.

Yan Z, Guo Z, Serbin SP, Song G, Zhao Y, Chen Y, Wu S, Wang J, Wang X, Li J, Wang B. 2021. Spectroscopy outperforms leaf trait relationships for predicting photosynthetic capacity across different forest types. *New Phytologist*. **232**:134-47.

Yu MH, Ding GD, Gao GL, Sun BP, Zhao YY, Wan L, Wang DY, Gui ZY. 2015. How the plant temperature links to the air temperature in the desert plant Artemisia ordosica. *PloS one* **10**: e0135452.

Zellweger F, De Frenne P, Lenoir J, Rocchini D, Coomes D. 2019. Advances in Microclimate Ecology Arising from Remote Sensing. *Trends in Ecology & Evolution* **34**: 327-341.

Zhou, S., Medlyn, B., Sabaté, S., Sperlich, D., & Prentice, I. C. 2014. Short-term water stress impacts on stomatal, mesophyll and biochemical limitations to photosynthesis differ consistently among tree species from contrasting climates. *Tree physiology*, **34**: 1035-1046.

834 **Table 1.** The source of environmental and trait data (grey zone) used for driving and evaluating a trait-based leaf energy balance model in

835 simulating T_{leaf} and ΔT at the Changbai (CB) and Xishuangbanna (XSBN) canopy crane sites.

Symbol	Description	Unit	Source	**Equipment/software**
T_{air}	Air temperature	℃	CB & XSBN sites	Weather station
u	Wind speed	m s^{-1}	CB & XSBN sites	Weather station
PAR	Photosynthetically active radiation	μmol m^{-2} s^{-1}	CB & XSBN sites	Weather station
RH	Relative humidity	--	CB & XSBN sites	Weather station
d	Leaf width	m	CB & XSBN sites	Image J
α_{PAR}	Absorptance of PAR band	--	CB & XSBN sites	SVC and PROSPECT
α_{NIR}	Absorptance of NIR band	--	CB & XSBN sites	SVC and PROSPECT
ε_{leaf}	Leaf emissivity	--	set as 0.95	--
$V_{c,max\ 25}$	Maximum carboxylation rate at 25℃	μmol m^{-2} s^{-1}	CB & XSBN sites	LI-COR 6400
g_1	Stomatal slope	--	PFT-specific [1]	--
T_{leaf}	Leaf temperature	℃	CB & XSBN sites	Thermal camera

836 [1] Lin *et al*. (2015).

837

Table 2. The source of environmental and trait data (grey zone) used to drive a trait-based leaf energy balance model through model sensitivity analysis respectively conducted at each forest site level.

Model input	Unit	Global range	Source
T_{air}	℃	--	CB, XSBN, PE sites
u	m s^{-1}	--	CB, XSBN, PE sites
PAR	μmol m^{-2} s^{-1}	--	CB, XSBN, PE sites
RH	--	--	CB, XSBN, PE sites
d	m	0.004-0.4	Wright *et al*. (2017)
α_{PAR}	m	0.73-0.96	Féret *et al*. (2017)
α_{NIR}	--	0.24-0.64	Féret *et al*. (2017)
ε_{leaf}	--	0.95-0.995	Chen *et al*. (2015)
$V_{c,max\ 25}$	μmol m^{-2} s^{-1}	13-163	Rogers (2014)
g_1	--	0.27-8.28	Lin *et al*. (2015)

Table 3. The source of environmental and trait data (grey zone) respectively used to derive modeled and field-observed trait-Δ*T* relationships.

Trait- Δ*T* relationship	Time	Model simulation		validation	
		Environment source	Global trait range	Environment source	Filed-measured trait and Δ*T*
Leaf size-Δ*T*	Midday	CB, XSBN, PE	0.004-0.4 m	CB, XSBN, PE	CB, XSBN, PE
PAR absorptance-Δ*T*	Midday	CB, XSBN	0.73-0.96	CB, XSBN	CB, XSBN
NIR absorptance-Δ*T*	Midday	CB, XSBN	0.24-0.64	CB, XSBN	CB, XSBN
$V_{c,max\ 25}$-Δ*T*	Midday	CB, XSBN	13-163 μmol m^{-2} s^{-1}	CB, XSBN	CB, XSBN
Leaf size-Δ*T*	Midnight	Literature [1] (New Zealand)	0.004-0.4 m	Literature [1] (New Zealand)	Literature [1] (New Zealand)

[1] Lusk & Clearwater (2015); Lusk *et al*. (2018).

Main Figures

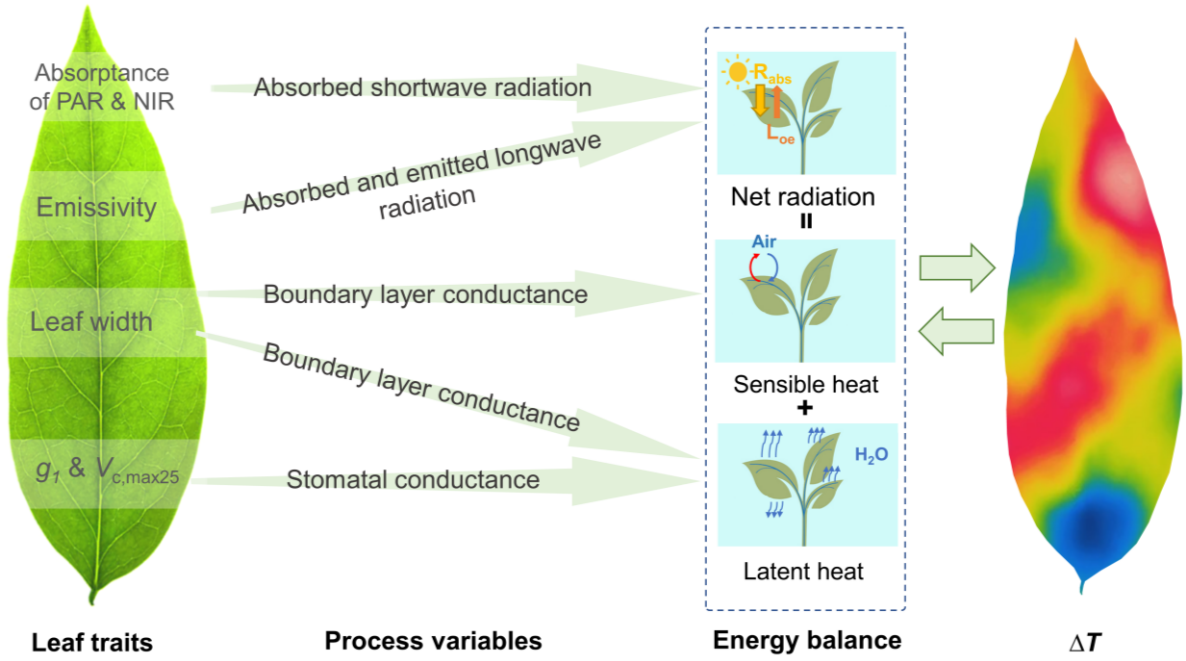

Figure 1. Theoretical pathways connecting leaf traits and associated process variables within the leaf energy balance equation that infers leaf-to-air temperature difference (ΔT). ΔT is determined by three energy fluxes (i.e. net radiation, sensible heat, and latent heat), which are further connected with the six leaf traits, including absorptance of PAR (α_{PAR}, 400-700nm), absorptance of NIR (700-2500nm), emissivity, leaf width, Medlyn-type stomatal slope (g_1) (Medlyn *et al.*, 2012), and maximum carboxylation capacity ($V_{c,max25}$).

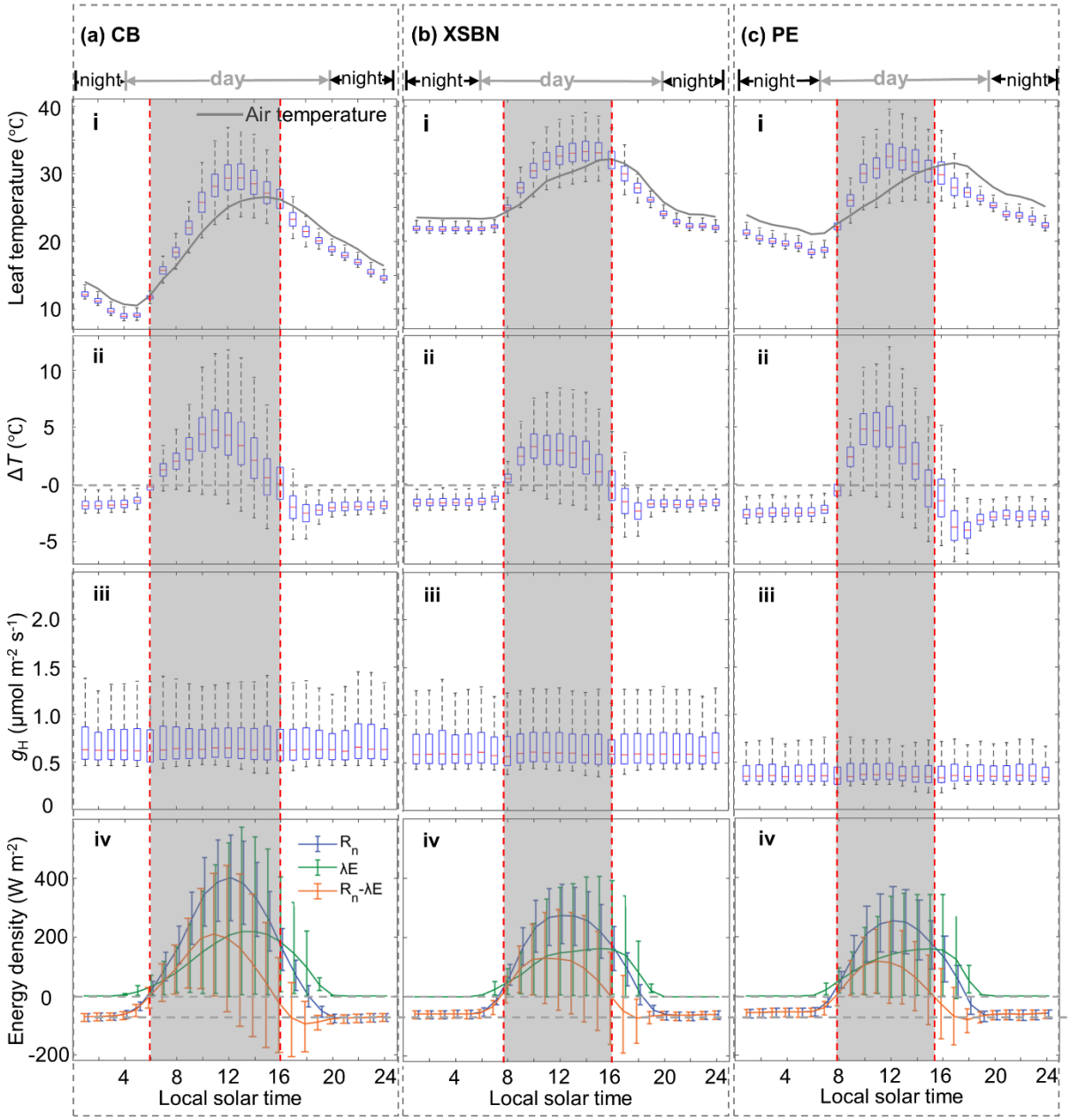

851

852 **Figure 2.** Diel variations in leaf temperature, air temperature, ΔT, and the associated three
853 state variables (i.e. g_H, R_n, and λE) were derived based on our trait-based leaf energy balance
854 model. Error bars indicate the ranges of maximum and minimum values of modeling results
855 associated with leaf traits at each given time of the day. The results are shown for three sites:
856 (a) CB, (b) XSBN, and (c) PE. The panels (i-iv) represent (i) modeled leaf temperature and
857 field-observed air temperature, (ii) modeled ΔT (modeled leaf temperature minus field-
858 observed air temperature), (iii) modeled heat boundary layer conductance of leaf (g_H), and (iv)
859 modeled net radiation flux (R_n), latent heat flux (λE) , and sensible heat flux (R_n - λE). Night-

time is defined as the period when PAR is less than 10 μmol m^{-2} s^{-1}. The grey zones in this figure indicate the time period when leaf temperature is higher than air temperature; the two red dash lines correspond to the time points when $R_n = \lambda E$ (also $T_{leaf} = T_{air}$).

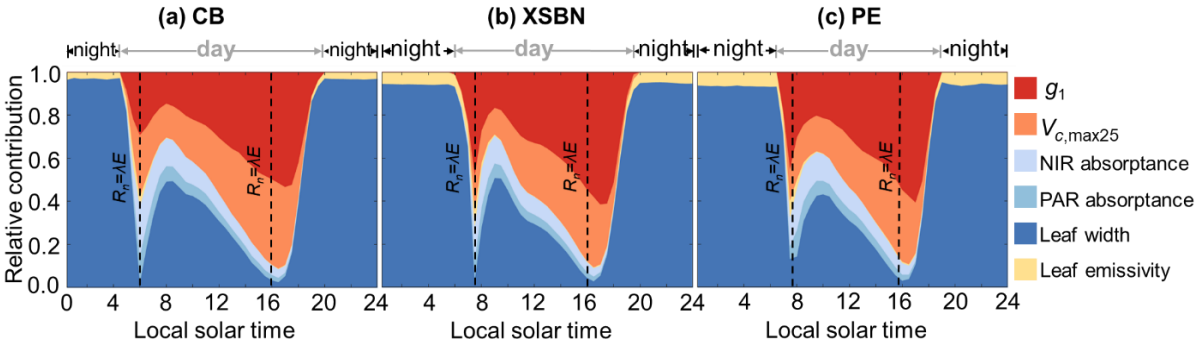

863

864 **Figure 3.** Diel variation in traits' relative contribution on regulating the Δ*T* variability. Night-
865 time is defined as the period when PAR is less than 10 μmol m^{-2} s^{-1}. The dashed lines in this
866 figure indicate the time points when net radiation flux (R_n) is equal to latent heat flux (λE)
867 (also see Fig. 2iv), during which leaf temperature is equal to air temperature and there is no
868 sensible heat exchange. The pattern is consistent for the three forest sites: (a) CB, (b) XSBN,
869 and (c) PE.

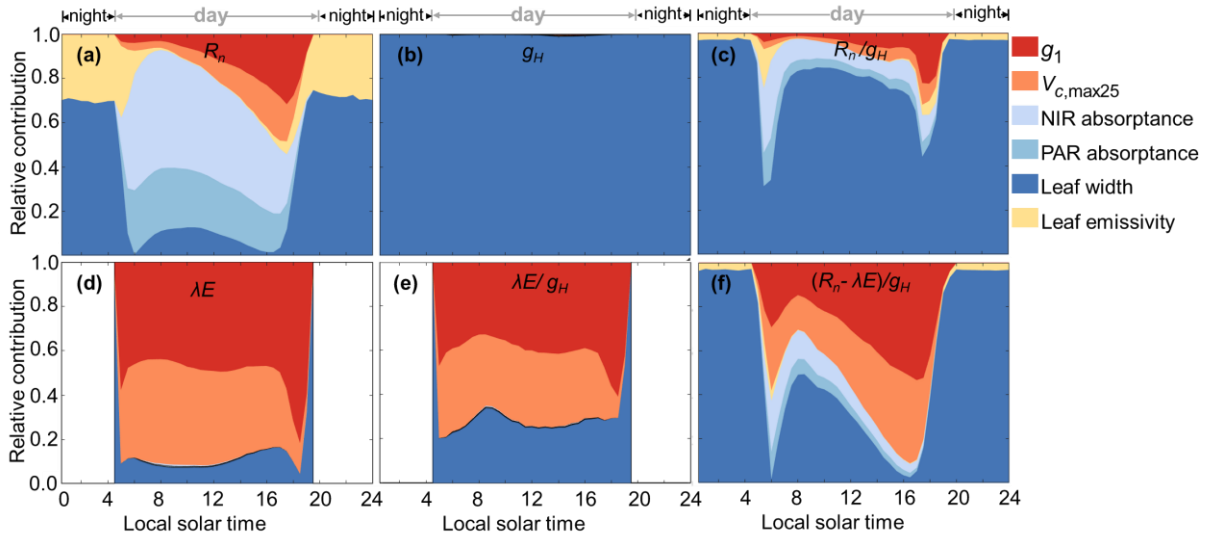

870

871 **Figure 4.** Diel variation in traits' relative contribution in regulating the three state variables
872 (i.e. R_n, g_H, and λE) that directly determine ΔT. The environmental variables from the CB site
873 (the same as that used in Fig. 3a) are used here to drive the trait-based leaf energy balance
874 model. The state variables of interest include (a) R_n, (b) g_H, (c) R_n/g_H, (d) λE, (e) $\lambda E/g_H$, and
875 (h) $(R_n-\lambda E)/g_H$. Night-time is defined as the period when PAR is less than 10 μmol m^{-2} s^{-1}.
876 Notably, the displayed relative contribution of leaf traits on $(R_n-\lambda E)/g_H$ is identical to traits'
877 relative roles on ΔT shown in Fig. 3a.

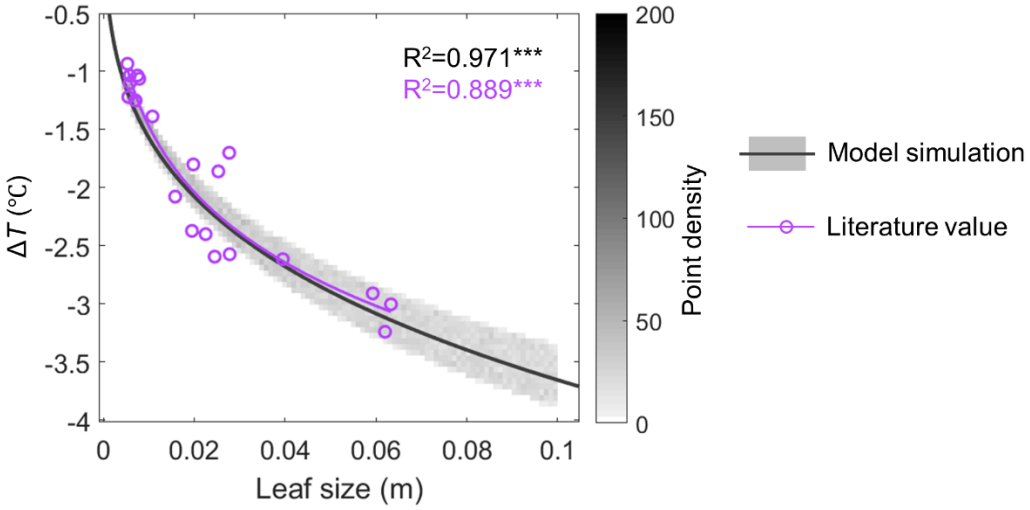

878

879 **Figure 5.** Modeled and field-based (derived from previous literature; solid purple circles)
880 relationship between leaf width and Δ*T* during night-time. The grey dots indicate the model-
881 derived leaf width-Δ*T* relationship under each random trait combination. The solid black line
882 marks the best fitted negative exponential relationship of leaf width-Δ*T* based on all the trait
883 combinations (*n*=2000). R^2 indicates the determination of coefficients, and *** indicates the
884 significance level of $p<0.001$ for the explored relationships.

885

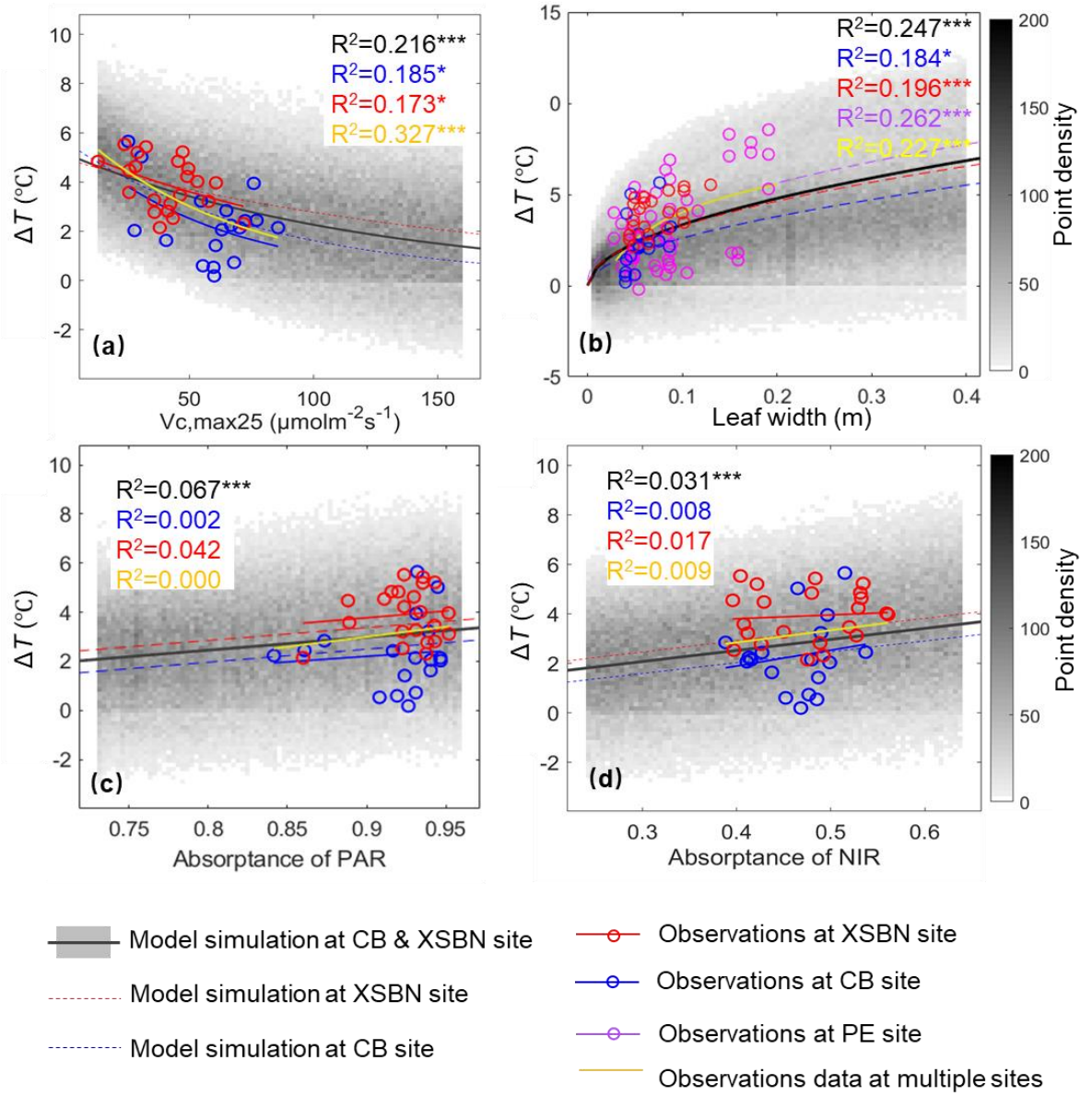

Figure 6. Modeled and field-based relationships between four leaf traits and ΔT during the noon-time (10:30 am-1:30 pm). Four leaf traits include (a) leaf maximum carboxylation rate scaled to 25℃ ($V_{c,max25}$), (b) leaf width, (c) the absorptance of PAR (α_{PAR}), and (d) the absorptance of NIR (α_{NIR}). The modeled results (grey dots for the simulation result under each random trait combination, and solid black lines/dashed color lines for corresponding best fitted relationships) are derived based on our trait-based leaf energy balance model. R^2 indicates the determination of coefficients, and two significant levels are used to indicate each relationship, including *** for p<0.001, and * for p<0.05.

Supporting Information

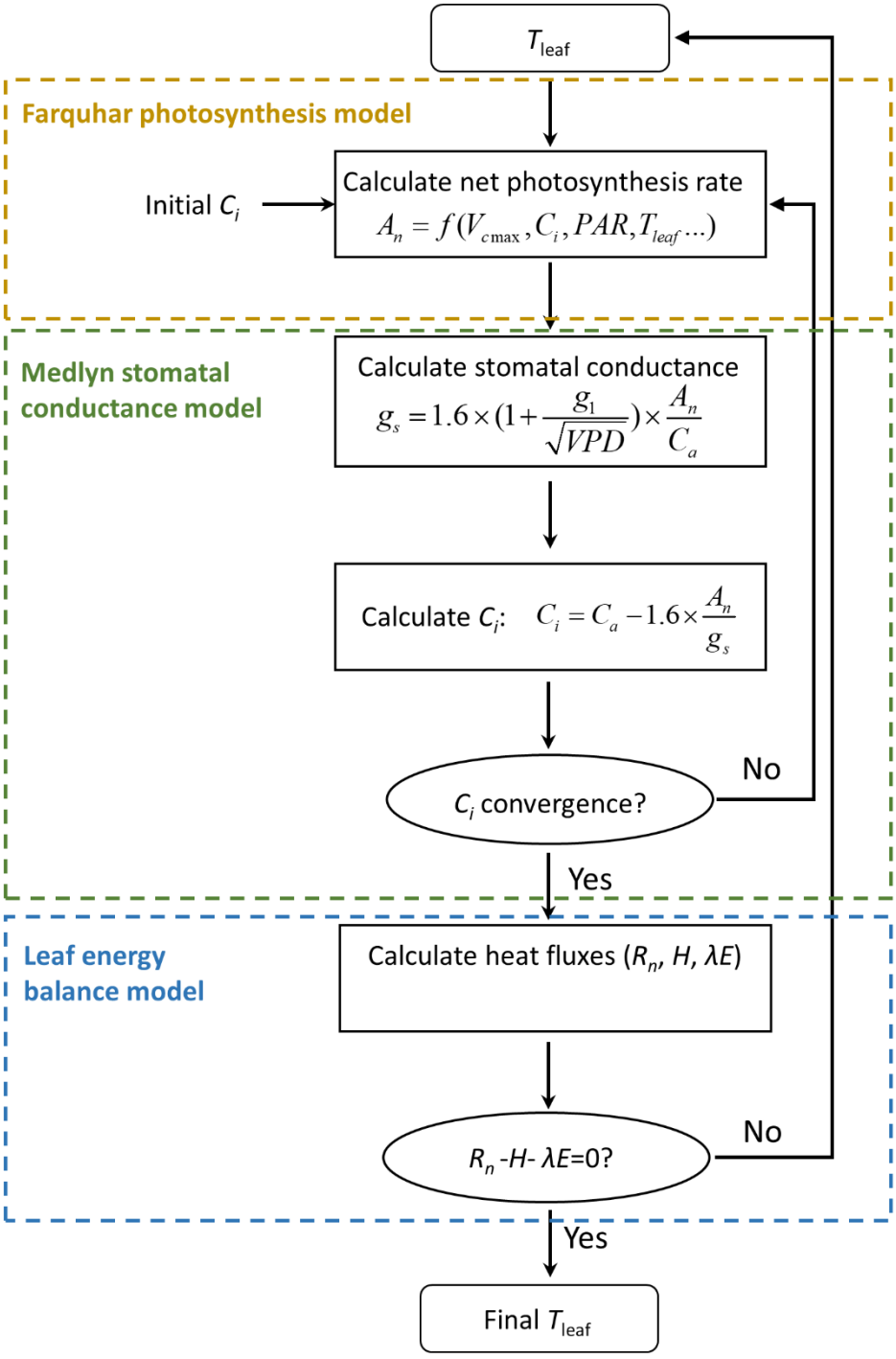

917

918 **Figure S1.** The flowchart of deriving leaf temperature (T_{leaf}) using a trait-based leaf energy
919 balance model that integrates a leaf energy balance model with a coupling of the FvCB-type
920 photosynthesis model (Farquhar *et al.*, 1980) and the Medlyn-type stomatal conductance
921 model (Medlyn *et al.*, 2011).

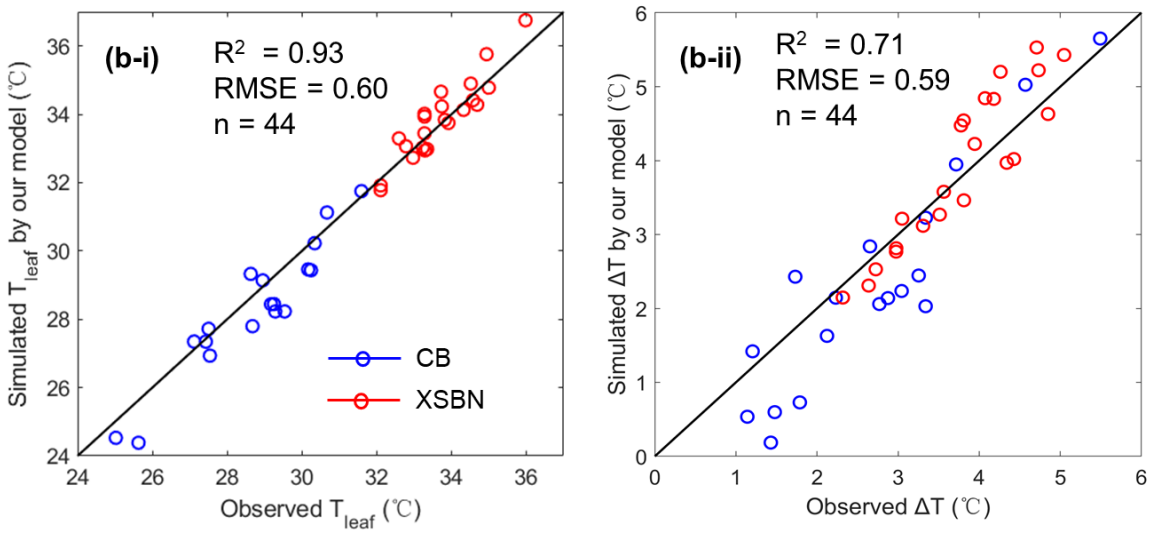

922

923 **Figure S2.** Evaluation of our modeling results with field observations, including (a) leaf
924 temperature (T_{leaf}) and (b) leaf-to-air temperature difference (ΔT). The model is driven by
925 field-derived leaf traits and *in-situ* measurements of environmental variables at the CB and
926 XSBN sites. The g_1 was set as constant (i.e. 4.64 for CB and 3.77 for XSBN) following Lin *et*
927 *al*. (2015). The solid line shows the 1:1 line. The R^2 and n represent the coefficient of
928 determination and total field observation size, respectively.

929

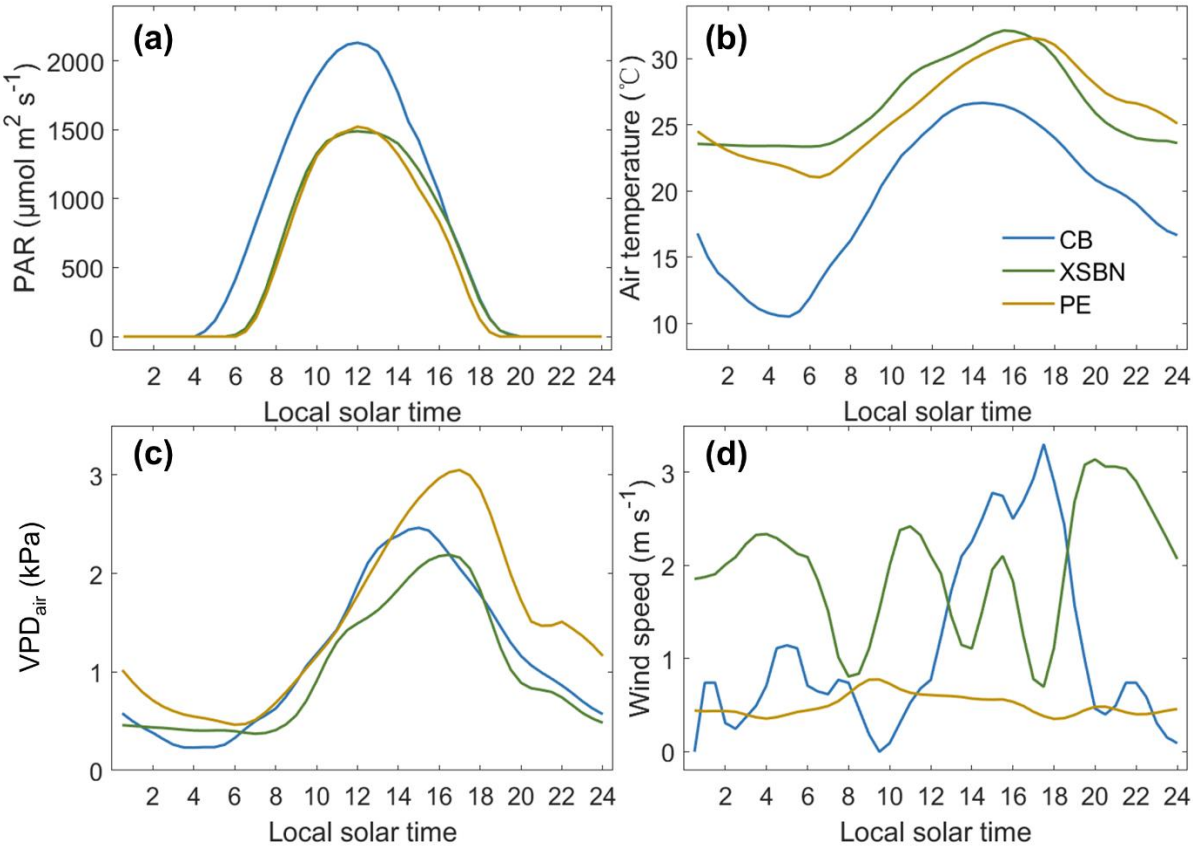

930

931 **Figure S3.** Diel patterns of key environmental variables at three forest sites, including (a)
932 photosynthetically active radiation (PAR), (b) air temperature, (c) vapour pressure deficit of
933 air (VPD_{air}), and (d) wind speed. These three forest sites include a high latitude temperate
934 forest at Mt. Changbai (CB) in Northern China, a tropical rainforest in Xishuangbanna
935 (XSBN) of Southern China, and a tropical dry forest in Pernambuco (PE) of Brazil.

936

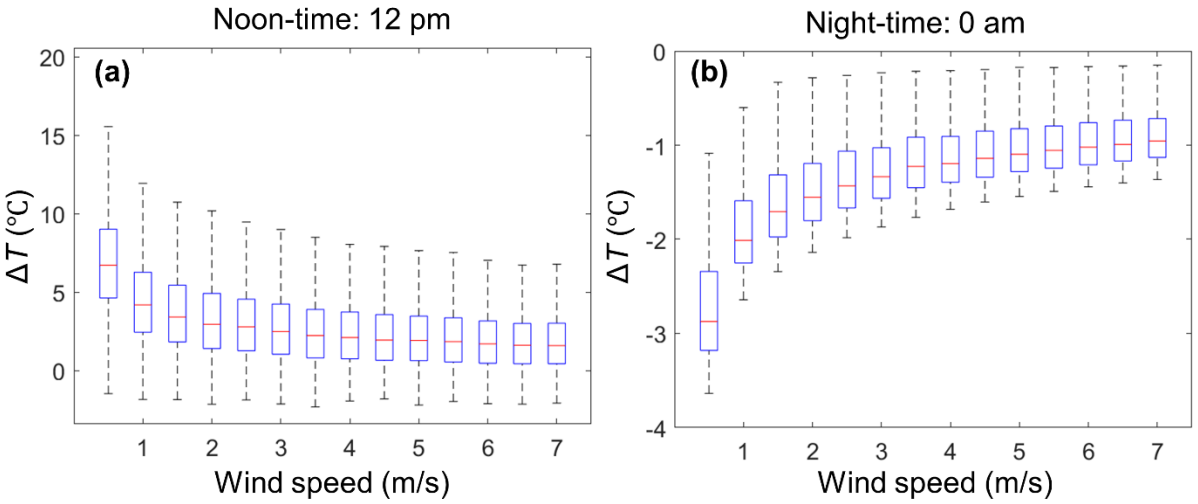

Figure S4. Assessing the impacts of wind speed on model-derived Δ*T* variability at both (a) noon-time (12 pm) and (b) midnight (0 am). The modeling results are based on an integration of the trait-based leaf energy balance model with field-measured environmental variables (except wind speed) under a clear-sky day of 2019-07-08 at the CB site, including the noon-time PAR=2115.0 μmol m^{-2} s^{-1}, T_{air}=25.5 ℃, and RH=35.7% and the night-time PAR=0.0 μmol m^{-2} s^{-1}, T_{air}=13.7 ℃, and RH=73.9%. The wind speed examined here ranges from 0.5 m s^{-1} to 7 m s^{-1} with an interval 0.5 m s^{-1}. Error bars indicate the ranges of maximum and minimum values of modeled Δ*T* associated with leaf traits at each given wind speed.

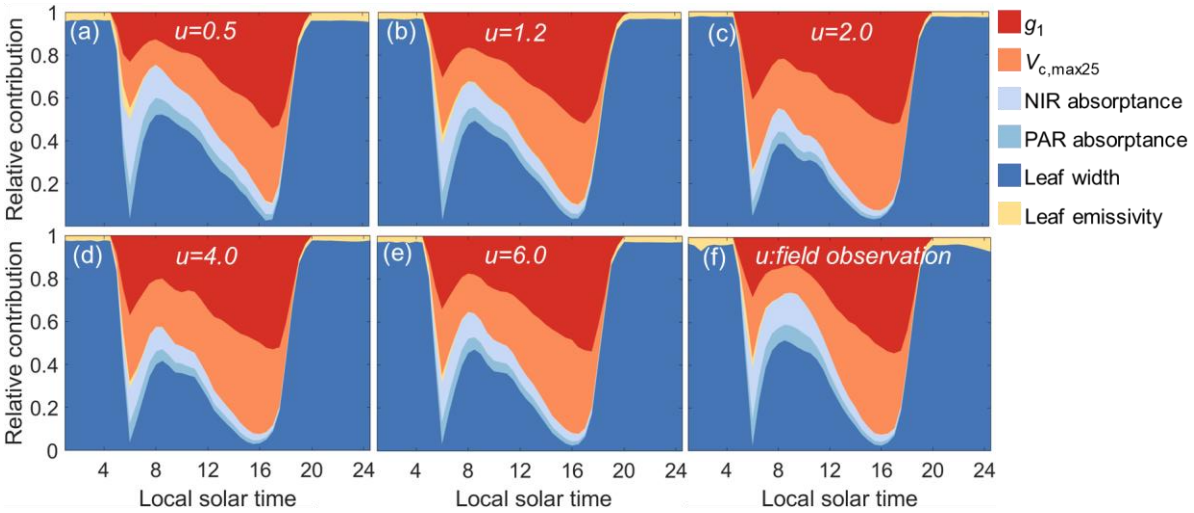

947

948 **Figure S5.** Assessing the impacts of different wind speed scenarios on model-derived traits'
949 relative contributions to the ΔT variability. Two types of wind speed settings are examined
950 here. First, wind speed is set as a constant value across the diel timescale, including (a) 0.5 m
951 s^{-1}, (b) 1.2 m s^{-1} (daily average), (c) 2.0 m s^{-1}, (d) 4.0 m s^{-1}, and (e) 6.0 m s^{-1}, respectively.
952 Second, wind speed is set as (f) *in-situ* measurements throughout the entire diel timescale
953 (also see Fig. S3d). The modeling results are based on an integration of the trait-based leaf
954 energy balance model with field-measured environmental variables (except wind speed)
955 under a clear-sky day of 2019-07-08 at the CB site, and the result shown in panel b is the
956 same as that shown in Fig. 3a.

957

958

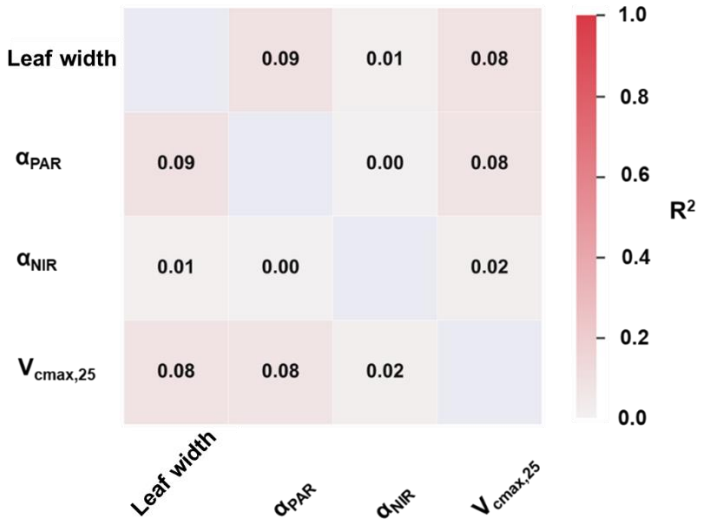

Figure S6. Heat map showing R^2 among four measured leaf traits (i.e. leaf size, PAR absorptance, NIR absorptance, and $V_{c,max25}$) at CB and XSBN sites.

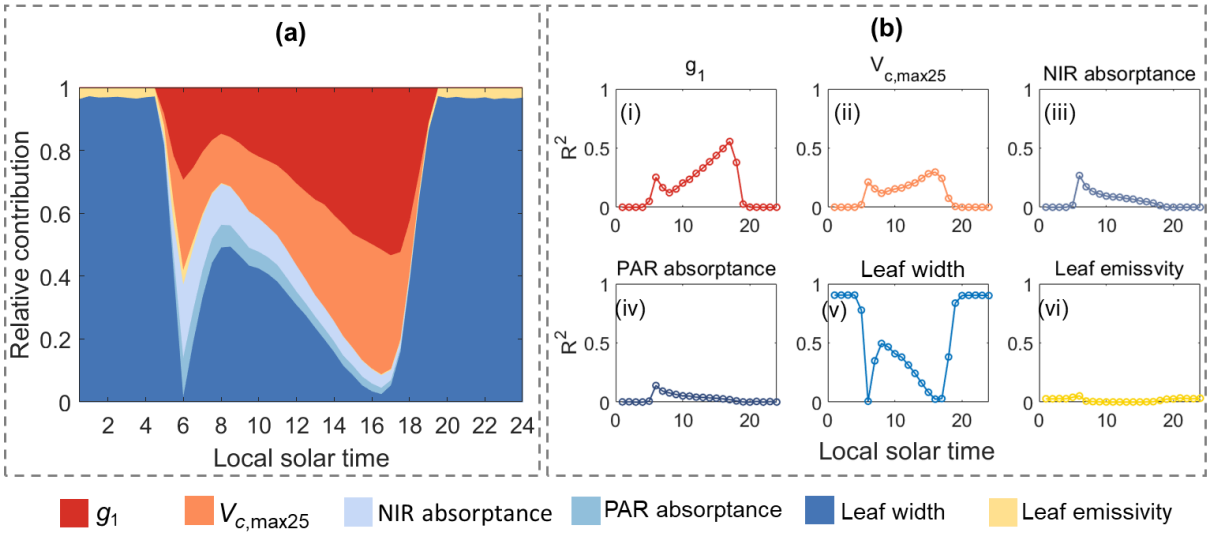

963

964 **Figure S7.** Diel patterns of traits' relative contribution on (a) ΔT and (b) trait-ΔT relationship.
965 The larger contribution of one trait on ΔT in panel (a), the larger R^2 between the trait and ΔT
966 in panel (b), which means a higher explanation of this trait on ΔT variation.

967

968

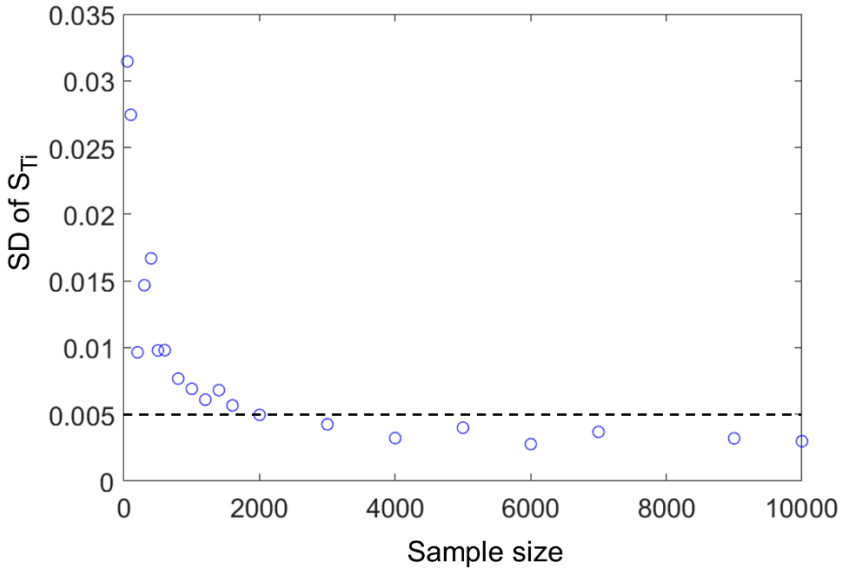

Figure S8. Changes in the standard deviation (SD) of total sensitivity index (S_{Ti}) with the sample size (*n*). S_{Ti} quantifies the proportion of model output variation explained by *n* and a larger S_{Ti} indicates higher sensitivity. It is calculated using the Jansen estimator (Jansen., 1999). The black dashed line indicates a 5‰ of the SD of S_{Ti}, below which the model sensitivity is stable.

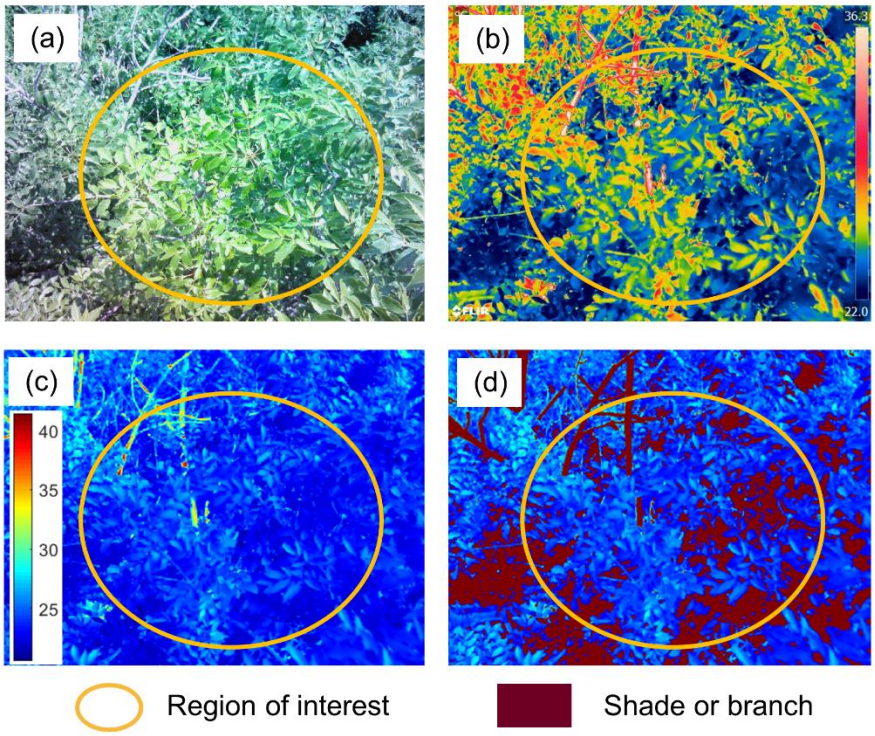

Figure S9. Example demonstration of deriving leaf temperature of canopy sunlit leaves from the thermal camera measurement. The *in-situ* thermal measurement of species *Fraxinus ornus* at the CB site on date 2019-07-03 is shown here for demonstration, and there are three steps for deriving leaf temperature. First, (a) a regular RGB photo, together with (b) a raw thermal photo, were simultaneously acquired using a thermal camera FLIR-T650sc (FLIR Systems AB, Taby, Sweden). Second, (c) the calibrated thermal photo is generated by calibrating the raw thermal photo with a R package of "ThermStats". Third, (d) the classified image is derived that differentiates sunlit leaves from the shaded leaves and branches in the calibrated thermal image using a supervised image classification. The yellow ellipse circles indicate the region of interest, and all the sunlit leaves pixels in the yellow ellipse of the calibrated thermal photo (i.e. panel c) are finally used to estimate leaf temperature of the target tree species.

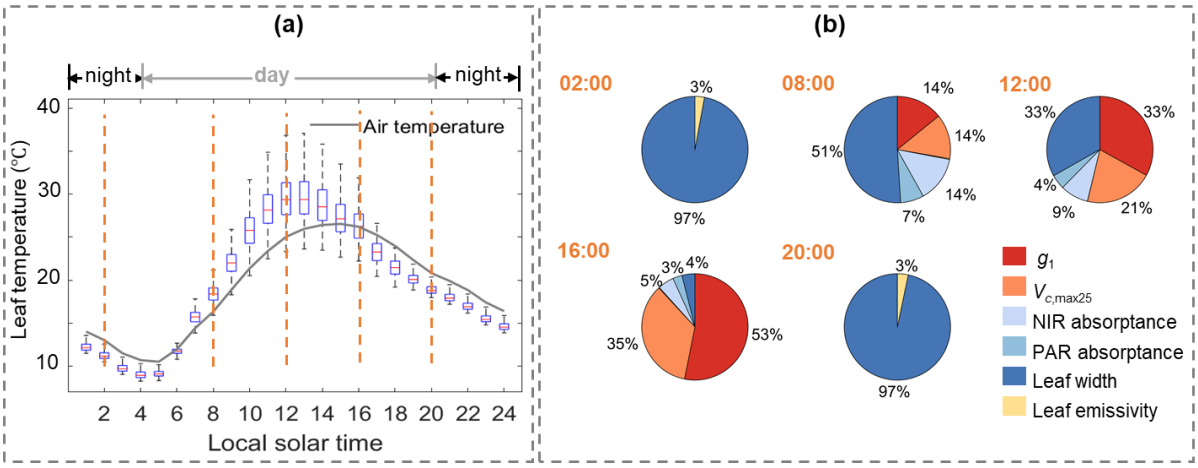

Figure S10. Leaf temperature variability and its drivers based on our model simulation. (a) Diel variations in leaf temperature, with error bars indicating the ranges of maximum and minimum values of modeling results associated with leaf traits at each given time of the day. (b) The drivers and their relative contributions to the leaf temperature variability at five given time points (corresponding to the orange lines in panel a).

Table S1. Summary of species and leaf traits of representative canopy trees across the three forest sites (i.e. CB, XSBN, and PE). The leaf traits include leaf width, PAR absorption, NIR absorption, and the maximum carboxylation rate of Rubisco standardized to 25℃ ($V_{c,\,max25}$). For each trait of a given species, data were used to calculate the mean trait value and the trait standard deviation (mean ± s.d.). The climatic conditions, approximated by mean annual temperature (MAT) and mean annual precipitation (MAP), are shown below for each site.

Site description	Specie name	Leaf width (cm)	PAR absorptance (unitless)	NIR absorptance (unitless)	$V_{c,max25}$ (μmol m^{-2} s^{-1})	# of trees	# of leaves
Site_name: CB	*Tilia amurensis*	5.40 ± 0.07	0.90 ± 0.01	0.41 ± 0.01	66.3 ± 6.1	4	13
	Quercus mongolica	6.48 ± 0.05	0.93 ± 0.02	0.46 ± 0.01	50.2 ± 10.4	2	6
location:	*Tilia mandshurica*	8.72 ± 0.08	0.94 ± 0.01	0.48 ± 0.01	74.5 ± 10.8	4	11
42°24′N, 128°06′E	*Fraxinus mandschurica*	4.09 ± 0.04	0.93 ± 0.01	0.49 ± 0.01	68.1 ± 13.0	2	5
	Acer pictum subsp. mono	7.62 ± 0.04	0.93 ± 0.01	0.52 ± 0.01	25.3 ± 2.6	1	3
MAT: 2.8ºC	*Phellodendron*	4.57 ± 0.05	0.94 ± 0.01	0.45 ± 0.01	35.6 ± 3.0	3	9
MAP: 691 mm	*Ulmus davidiana*	4.00 ± 0.05	0.92 ± 0.01	0.48 ± 0.01	59.6 ± 5.8	3	9
	Parashorea chinensis	4.84 ± 0.00	0.89 ± 0.01	0.44 ± 0.01	31.3 ± 4.7	4	12
	Alseodaphne petiolaris	10.20 ± 0.10	0.94 ± 0.01	0.48 ± 0.02	35.9 ± 4.4	3	9
	Sapium baccatum	9.30 ± 0.15	0.95 ± 0.01	0.55 ± 0.02	54.0 ± 7.8	2	6
	Colona thorelii	6.00 ± 0.02	0.92 ± 0.02	0.40 ± 0.01	53.6 ± 12.0	2	6
Site_name: XSBN	*Castanopsis indica*	6.40 ± 0.05	0.94 ± 0.01	0.49 ± 0.01	71.8 ± 14.0	2	6
	Schefflera bodinieri	5.50 ± 0.06	0.92 ± 0.01	0.53 ± 0.01	49.1 ± 14.0	1	3
Location:	*Sloanea tomentosa*	5.00 ± 0.04	0.92 ± 0.01	0.48 ± 0.01	13.2 ± 2.8	1	3
21°47′N, 101°03′E	*Pometia pinnata*	6.75 ± 0.04	0.93 ± 0.01	0.53 ± 0.01	28.2 ± 4.2	2	5
	Litsea dilleniifolia	13.00 ± 0.08	0.92 ± 0.01	0.40 ± 0.01	23.8 ± 4.2	1	3
MAT: 21.8ºC	*Duabanga grandiflora*	8.57 ± 0.06	0.93 ± 0.01	0.56 ± 0.01	53.2 ± 6.3	1	3
MAP: 1493 mm	*Ficus langkokensis*	4.43 ± 0.04	0.93 ± 0.01	0.41 ± 0.01	53.2 ± 6.3	2	6
	Lithocarpus grandifolius	6.40 ± 0.08	0.94 ± 0.01	0.49 ± 0.01	41.3 ± 9.7	1	2
	Lithocarpus craibianus	6.00 ± 0.15	0.92 ± 0.01	0.53 ± 0.01	45.4 ± 6.2	1	2
	Diospyros atrotricha	8.50 ± 0.07	0.95 ± 0.01	0.53 ± 0.01	42.3 ± 7.9	2	5
	Croton conduplicatus	2.89 ± 0.00	—	—	—	2	4
	Jathropa mollissima	15.80 ± 0.14	—	—	—	2	3

	Commiphora leptophloeos	5.42 ± 0.04	—	—	—	2	3
Site_name: PE	*Cnidoscolus quercifolius*	4.06 ± 0.04	—	—	—	1	2
	Schinopsis brasiliensis	6.10 ± 0.08	—	—	—	3	5
Location:	*Senegalia piauhiensis*	7.44 ± 0.06	—	—	—	3	5
9°03′S, 40°19′W	*Sapium glandulosum*	4.05 ± 0.05	—	—	—	2	4
	Poincianella microphylla	3.30 ± 0.04	—	—	—	2	4
MAT: 26.2ºC	*Pseudobombax simplicifolium*	4.40 ± 0.05	—	—	—	2	5
MAP: 510 mm	*Bauhinia cheilantha*	6.46 ± 0.05	—	—	—	2	3
	Manihot pseudoglaziovii	10.44 ± 0.12	—	—	—	2	4
	Handroanthus spongiosus	6.82 ± 0.08	—	—	—	2	4
	Varronia leucocephala	0.22 ± 0.05	—	—	—	2	3

1002

Table. S2. The equations of leaf energy balance model.

Equations	Definition	No.	Ref.
$R_n = H + \lambda E$	Leaf energy balance equation (W m^{-2})	1	A, B
$R_n = R_{abs} - L_{oe}$	Net radiation flux (W m^{-2})	2	A, B
$R_{abs} = (\alpha_{PAR} R_{PAR} + \alpha_{NIR} R_{NIR})(1+\rho) + \alpha_L \sigma(\varepsilon_{sky} T_{sky}^4 + \varepsilon_{sur} T_{sur}^4)$	Absorbed radiation flux of leaf (W m^{-2})	3	A, B
$L_{oe} = 2\varepsilon_{leaf} \sigma T_{leaf}^4$	Emitted radiation flux of leaf (W m^{-2})	4	A, B
$H = 2 * c_p g_H (T_{leaf} - T_{air})$	Sensible heat (convection) flux (W m^{-2})	5	A, B
$g_H = g_{H,free} + 1.4 \times g_{H,forced}$	Heat boundary conductance (mol m^{-2} s^{-1})	6	A, C
$g_{H,forced} = \frac{0.664 \hat{\rho} D_H \mathrm{Re}^{1/2} \mathrm{Pr}^{1/3}}{d}$	Forced convection conductance of heat (mol m^{-2} s^{-1})	7	A, C
$g_{H,free} = \frac{0.54 \hat{\rho} D_H (Gr \mathrm{Pr})^{1/4}}{d}$	Free convection conductance of heat (mol m^{-2} s^{-1})	8	A, C
$\mathrm{Re} = \frac{ud}{v}$	Reynolds number: Ratio of inertial viscous forces	9	A
$\mathrm{Pr} = \frac{v}{D_H}$	Prandtl number: Ratio of kinematic viscosity to thermal diffusivity	10	A
$Gr = \frac{g d^3 \Delta T}{(T_{air} + 273.15) v^2}$	Grashof number: Ratio of a buoyant force times an inertial force to the square of a viscous force	11	A
$\lambda E = \lambda g_v (e_s(T_{leaf}) - e(T_{air})) / P_a$	Latent heat (transpiration) flux (mol m^{-2} s^{-1})	12	A
$g_v = \frac{1}{\frac{1}{g_s} + \frac{1}{g_b}} = \frac{g_s g_b}{g_s + g_b}$	Water vapor conductance (mol m^{-2} s^{-1})	13	A
$g_b = g_{b,free} + 1.4 \times g_{b,forced}$	Boundary layer conductance of water vapor (mol m^{-2} s^{-1})	14	A, C
$g_{b,forced} = \frac{0.664 \hat{\rho} D_j \mathrm{Re}^{1/2} Sc^{1/3}}{d}$	Forced convection conductance of vapor (mol m^{-2} s^{-1})	15	A
$g_{b,free} = \frac{0.54 \hat{\rho} D_j (GrSc)^{1/4}}{d}$	Free convection conductance of vapor (mol m^{-2} s^{-1})	16	A
$Sc = \frac{v}{D_j}$	Prandtl number: Ratio of kinematic viscosity to mass diffusivity	17	A
$e_s(T) = 0.6108 \times \exp(\frac{17.269T}{237.2+T})$	Saturated vapor pressure at T ℃ (kPa)	18	A, D
$e(T) = e_s(T) \times RH$	Vapor pressure at T ℃ (kPa)	19	A

Relevant references: A: Campbell & Norman (2012); B: Jones, (2013); C: Huang *et al.* (2015); and D: Murray (1967).

Table S3. The equations of FvCB-type leaf photosynthesis model (Farquhar *et al*., 1980), and the Medlyn-type stomatal conductance model (Medlyn *et al*., 2011).

Equations	Definition	No.	Ref.
$A_n = min\left\{A_c, A_j, A_s\right\} - R_l$	Leaf level net assimilation rate (μmol CO_2 m^{-2} s^{-1})	1	E
$A_c = max\{V_{cmax} \times \frac{C_i - \Gamma_*}{C_i + K'}, 0\}$	Rubisco-limited photosynthesis (μmol CO_2 m^{-2} s^{-1})	2	E
$K' = K_C \times (1 + \frac{O}{K_O})$	Effective Michaelis-Menten Constant	3	E
$A_j = \max\{J \times \frac{C_i - \Gamma_*}{4 \times (C_i + 2 \times \Gamma_*)}, 0\}$	Electron-transport limited rate of photosynthesis (μmol CO_2 m^{-2} s^{-1})	4	E
$J_e = \Phi_{PSII,\max} \times \alpha \times \beta \times Q$	The rate of whole electron transport (μmol m^{-2} s^{-1})	5	G
$J = \frac{J_e + J_{\max} - \sqrt{(J_e + J_{\max})^2 - 4 \times \Theta \times J_e \times J_{\max}}}{2 \times \Theta}$	The rate of electrons through the thylakoid membrane (μmol CO2 m^{-2} s^{-1})	6	E
$A_s = 0.5 \times V_{c\max}$	Triose phosphate export limited rate of photosynthesis (μmol CO_2 m^{-2} s^{-1})	7	F
$Parameter = Parameter_{25} \times exp\frac{(T_K - 298) \times \Delta H_a}{R \times T_K \times 298}$	Temperature functions for parameters that are based on Rubisco kinetic properties and do not have an optimum within a biologically significant temperature range (K_C, K_O, Γ^*, R_l, and in most cases $V_{c,max25}$)	8	G
$J_{\max} = J_{\max 25} \times \frac{e^{-(\frac{T_L - Topt}{\Omega_T})}}{e^{-(\frac{25 - Topt}{\Omega_T})}}$	Temperature function for maximum electron transport rate, J_{max}	9	G, H
$\Omega_T = 11.6 + 0.18 \times T_{opt}$	The coefficient for temperature function of J_{max}	10	G, H
$J_{\max 25} = 1.67 \times V_{c\max 25}$	Linear scaling relationship between J_{max25} and $V_{c,max25}$	11	I, J
$T_K = T_l + 273.15$	Leaf temperature in Kelvin	12	G
$R_{l25} = 0.015 \times V_{c\max 25}$	Leaf dark respiration at 25℃ (μmol CO_2 m^{-2} s^{-1})	13	I
$g_s = 1.6 \times (1 + \frac{g_1}{\sqrt{VPD}}) \times \frac{A_n}{C_a}$ $A_n = g_s \times (C_a - C_i)$ $\Rightarrow C_i = C_a \times (1 - \frac{1}{1.6 \times (1 + \frac{g_1}{\sqrt{VPD}})})$	Use the optimal stomatal model to estimate internal CO_2 concentration (C_i) from atmospheric CO_2 concentration (C_a) and vapor pressure deficit (VPD)	14	K

Relevant references: E: Farquhar *et al*. (1980); F: Ryu *et al*. (2011); G: Bernacchi *et al*. (2013); H: June *et al*. (2004); I: Bonan *et al*. (2014); J: Wu *et al*. (2017); and K: Medlyn *et al*. (2011).

1011

Table S4. Variables, parameters, and associated descriptions used in the trait-based leaf energy balance model.

Model	Symbols	Definition	Values	Ref.
Leaf energy balance model	d	Leaf width (m)	0.004-0.4	L
	ε_{leaf}	Leaf emissivity	0.95-0.995	M
	α_{PAR}	Leaf absorptance at the visible band (400-700nm)	0.73-0.96	N
	α_{NIR}	Leaf absorptance at NIR band (700-2500nm)	0.24-0.64	N
	PAR	Photosynthetically active radiation	observation	-
	u	Wind speed (m s^{-1})	observation	-
	RH	Relative humidity (%)	observation	-
	T_{air}	Air temperature (℃)	observation	-
	ε_{sur}	Emissivity of the surrounding underside leaf		
	Initial T_{leaf}	Initial Leaf temperature (=T_{air}) (℃)	Same as T_{air}	-
	c_p	Heat capacity of air (J mol^{-1} K^{-1})	29.3	A
	α_L	Leaf absorptance at long-wave band (>3000nm)	Same as ε_{leaf}	M
	ρ	The reflectivity of surrounding leaf	0.13	A, B
	$\hat{\rho}_{20}$	Molar density of air at 20 ℃ (mol m^{-3})	41.6	A, B
	σ	Stefan–Boltzmann constant (W m^{-2} K^{-4})	5.6703×10^{-8}	A, B
	g	Gravitational acceleration (m s^{-1})	9.8	A, B
	λ	Latent heat of vaporization of water (J mol-1)	44000	A, B
	$D_{H,20}$	Diffusion coefficient of heat in air at 20 ℃ (mm^2 s^{-1})	21.4	A, B
	R	Gas constant (J mol^{-1} K^{-1})	8.3143	A, B
	Pa	Standard atmospheric pressure (kPa)	101.325	A, B
Photosynthesis model	C_a	Ambient CO_2 concentration (μmol mol^{-1})	380	E
	Initial C_i	Initial intercellular CO_2 concentration (=0.7*C_a; μmol mol^{-1})	266	E
	O	Oxygen concentration (mmol mol-1)	205	E
	β	Fraction of photosystem II to photosystem I	0.5	E, G
	$\Phi_{PSII,\ max}$	Maximum quantum efficiency of PSII photochemistry	0.7	G
	Θ	Curvature term	0.7	E, I
	$V_{cmax,25}$	Maximal carboxylation rate at 25°C (μmol m^{-2} s^{-1})	13-163	O
	T_{opt}	Optimal leaf temperature for J_{max} (°C)	35	P
Stomatal conductance model	g_1	Stomatal conductance slope	0.27-8.28	Q
	VPD_{leaf}	leaf-to-air vapour pressure deficit (= e_s (T_{leaf})-e(T_{air}); kPa)	Calculation	E, F
	A_n	Net assimilation rate (μmol m^{-2} s^{-1})	Calculation	E
	C_a	Ambient CO_2 concentration (μmol mol^{-1})	380	E
	Initial C_i	Initial intercellular CO_2 concentration (=0.7*Ca; μmol mol^{-1})	266	E

Relevant references: L: Wright *et al*. (2017); M: Chen *et al*. (2015); N: Féret *et al*. (2017); O: Rogers *et al*. (2014); P: Lloyd & Farquhar (2008); and Q: Lin *et al*. (2015).

Relevant references for Tables S1-S3

[A] **Campbell GS, Norman J. 2012.** *An introduction to environmental biophysics*: Springer Science & Business Media.

[B] **Jones HG. 2013.** *Plants and microclimate: a quantitative approach to environmental plant physiology*. Cambridge university press.

[C] **Huang CW, Chu CR, Hsieh CI, Palmroth S, Katul GG. 2015.** Wind-induced leaf transpiration. *Advances in Water Resources* **86**: 240-255.

[D] **Farquhar GD, von Caemmerer Sv, Berry JA. 1980.** A biochemical model of photosynthetic CO2 assimilation in leaves of C 3 species. *Planta* **149**: 78-90.

[E] **Murray FW. 1967.** On the computation of saturation vapor pressure. *J. Appl. Meteorol* **6**: 203-204.

[F] **Ryu Y, Baldocchi DD, Kobayashi H, Van Ingen C, Li J, Black TA, Beringer J, Van Gorsel E, Knohl A, Law BE et al. 2011.** Integration of MODIS land and atmosphere products with a coupled- process model to estimate gross primary productivity and evapotranspiration from 1 km to global scales. *Global Biogeochemical Cycles* **25**: GB4017.

[G] **Bernacchi CJ, Bagley JE, Serbin SP, RUIZ‐VERA UM, Rosenthal DM, & Vanloocke A. 2013**. Modeling C3 photosynthesis from the chloroplast to the ecosystem. *Plant, Cell & Environment* **36:** 1641-1657.

[H] **June T, Evans JR, Farquhar GD.** 2004. A simple new equation for the reversible temperature dependence of photosynthetic electron transport: a study on soybean leaf. *Functional plant biology* **31**: 275-283.

[I] **Bonan GB, Williams M, Fisher R A, & Oleson K W. 2014.** Modeling stomatal conductance in the earth system: linking leaf water-use efficiency and water transport along the soil-plant-atmosphere continuum. *Geoscientific Model Development* **7**: 2193-2222.

[J] **Wu J, Serbin SP, Xu X, Albert LP, Chen M, Meng R, Saleska SR, Rogers A. 2017.** The phenology of leaf quality and its within- canopy variation is essential for accurate modeling of photosynthesis in tropical evergreen forests. *Global Change Biology* **23**: 4814-4827.

[K] **Medlyn BE, Duursma RA, Eamus D, Ellsworth DS, Prentice IC, Barton CV, Crous KY, De Angelis P, Freeman M, Wingate L. 2011.** Reconciling the optimal and

empirical approaches to modeling stomatal conductance. *Global Change Biology* **18**: 3476-3476.

[L] **Wright IJ, Dong N, Maire V, Prentice IC, Westoby M, Díaz S, Gallagher RV, Jacobs BF, Kooyman R, Law EA et al. 2017.** Global climatic drivers of leaf size. *Science* **357**: 917-921.

[M] **Chen C. 2015.** Determining the leaf emissivity of three crops by infrared thermometry. *Sensors* **15**: 11387-11401.

[N] **Rogers A. 2014.** The use and misuse of Vc,max in Earth System Models. *Photosynthesis research* **119**: 15-29.

[O] **Rogers A. 2014.** The use and misuse of Vc,max in Earth System Models. *Photosynthesis research* **119**: 15-29.

[P] **Lloyd J, Farquhar GD. 2008.** Effects of rising temperatures and [CO2] on the physiology of tropical forest trees. *Philosophical Transactions of the Royal Society B: Biological Sciences* **363**: 1811-1817.

[Q] **Lin YS, Medlyn BE, Duursma RA, Prentice IC, Wang H, Baig S, Eamus D, De Dios VR, Mitchell P, Ellsworth DS et al. 2015.** Optimal stomatal behaviour around the world. *Nature Climate Change* **5**: 459-464.

Supporting Method S1.

Field measurements of environmental variables, leaf traits, and ΔT

Environmental variables

For the sites of CB and XSBN, we measured environmental variables with a mobile weather station (WatchDog 2550, Spectrum Technologies Inc., Aurora, IL), which was installed on the top of the canopy crane tower on the day 1 of field measurements. The weather station recorded environmental variables at half an hour interval continuously for approximately two weeks until the end of field campaigns at each site. Environmental measurements include T_{air}, PAR, RH, and u (Fig. S3). VPD_{air} was derived using the formula proposed by Murray (1967) (Equation 18 of Table S2) with field-measured T_{air} and RH as input. Since T_{air} could be more dynamic under the mixed cloudy-sunny days, in order to minimize such impacts, we only used environmental measurements from clear-sky days, including environmental measurements of 2019-07-08 for CB and of 2019-08-10 for XSBN. Notably, we interpolated the T_{air} from half-hour intervals to 1-minute intervals using spline interpolation method (de Boor., 1978), which allowed us obtain the T_{air} at the time of T_{leaf} record to calculate ΔT (see section *Leaf temperature and* ΔT). Additionally, to minimize the impacts of rapid fluctuations of wind speed on causing T_{leaf} variability, we set the wind speed as daily averages for the model input, which is 1.2 m s^{-1} for CB and 1.0 m s^{-1} for XSBN.

At the PE site, environmental variables were accessed from a local eddy flux tower belonging to Embrapa Semiárido, Brazil. The measurements were recorded at half an hour interval, and included T_{air}, PAR, RH, and u (Fig. S3). VPD_{air} was calculated using the same approach mentioned above. Environmental measurements of a clear-sky day (2018-04-16), representing the central time period of field campaigns at this site, were used to drive our trait-based leaf energy balance model. For the same reason, to minimize rapid fluctuating wind speed effects, we set the wind speed to the daily average of 0.5 m s^{-1}.

Leaf gas exchange and $V_{c,max25}$

At the CB and XSBN sites, leaf gas exchange was measured using three portable gas exchange systems (LI-6400XT; Li-COR Inc., Lincoln, NE, USA). The response of A_n to the intercellular CO_2 concentration (C_i), commonly known as A-C_i curves, were measured on the sunlit leaves from the detached branches of top canopy trees. These branches were cut in water before dawn using the canopy crane to avoid xylem embolism (Wu *et al.*, 2020). And

then, the branches were stored in individual water buckets, and kept in deep shade until used for measurements. For each selected canopy tree, we randomly sampled two branches and measured the A-C_i curves of 1-3 leaves per branch, closely following the protocol of Rogers *et al.*, (2017). We set the gradient of reference CO_2 concentration as follows: 400, 325, 250, 175, 100, 66, 33, 400, 400, 400, 475, 575, 675, 800, 1000, 1400, 1800, 400 μmol mol^{-1}. The leaf was put under 400 μmol CO_2 mol^{-1} for photosynthetic stabilization before the *A-Ci* curve measurements. During the measurements, T_{leaf} was set to ambient air temperature or 1-2 ℃ above the dew point to avoid condensation inside the leaf chamber, and RH was set to 50-85%. The saturated PAR at CB and XSBN was set to 1700 μmol m^{-2} s^{-1} and 2000 μmol m^{-2} s^{-1}, respectively, based on the preliminary light response curves and previous empirical studies in these biomes (Croft *et al*., 2017; Wu *et al.*, 2019). A biochemical photosynthesis model (Farquhar *et al*., 1980) was then used to fit the A-C_i curves, by which we derived the leaf maximum carboxylation capacity ($V_{c,max}$) using the same code developed in Wu *et al*. (2019). Finally, we standardized $V_{c,max}$ to a reference temperature of 25℃ ($V_{c,max25}$) using the same kinetic constants and temperature response functions as Bernacchi *et al*. (2013).

Leaf absorptance for visible and near-infrared light

At the CB and XSBN sites, leaf absorptance for visible (400-700 nm; α_{PAR}) and near-infrared (700-2500 nm; α_{NIR}) light were derived based on the inversion of leaf reflectance spectra using a process-based model (i.e. PROSPECT; Jacquemoud & Baret, 1990; Féret *et al*., 2017), following Wu *et al*. (2018). It includes two steps. First is the measurements of leaf reflectance spectra. Upon finishing the gas exchange measurements, leaves were immediately measured for leaf reflectance spectra using a portable spectroradiometer SVC HR-1024i (i.e. Spectra Vista Corporation Inc., Poughkeepsie, NY, USA; spectra full-range: 350-2500nm), following the standard procedure (Wu *et al*., 2019). Specifically, the fiber optic probe (SVC LC-RP-Pro) with an internal calibrated light source was used together with a black background for leaf reflectance measurements. For each leaf, reflectance spectra were measured on 3-6 different parts of the leaf adaxial surface, and then averaged to determine the mean reflectance spectra across all wavelengths.

Second is the model inversion to derive leaf absorptance. With the measurements of leaf reflectance spectra, we next estimated leaf transmittance and subsequent absorptance by inverting the PROSPECT model after it was optimized to match field measurements of leaf reflectance spectra. We used the PROSPECT model because this model is process-based, and

the model-inverted leaf absorptance has been shown with high consistency compared with the values obtained with an integrating sphere for fresh leaves (Shiklomanov *et al.*, 2016; Wu *et al.*, 2018). We here used the same inversion code as Wu *et al.* (2018) to derive the PROSPECT-inverted leaf absorptance, and then combined the spectral response function for visible (400-700 nm) and near-infrared (700-2500 nm) light to respectively derive α_{PAR} and α_{NIR}.

Leaf temperature and ΔT

At the CB and XSBN sites, leaf temperature of sunlit upper canopy foliage was measured using a thermal camera FLIR-T650sc (FLIR Systems AB, Taby, Sweden; spectral wavelength range: 7.5-13.0 μm), which was held about 1-m directly above the treetop accessed by the canopy crane facility (see example RGB and thermal photos in Fig. S8a&b). These thermal measurements were conducted under clear-sky days between 10:30 am to 1:30 pm local time of each site. With the FLIR-T650sc thermal camera, two unshaded branches in the canopy top and representative of each canopy tree were selected for thermal measurements. For each thermal measurement, we generated two images, including one RGB image (with a resolution of 2592*1944 pixels; e.g. Fig. S8a) and one raw thermal image (with a resolution of 640*480 pixels; e.g. Fig. S8b). In order to obtain the surface temperature of leaves, we converted these raw thermal images into the calibrated digital grey image using the R package 'ThermStats' (Senior *et al.*, 2019), where the digital grey values in the calibrated images (leaf emissivity was set to 0.95) indicates the corresponding T_{leaf} readings. Additionally, since our main focus was on sunlit leaves, we developed a supervised classification approach to differentiate the sunlit leaves from other backgrounds (i.e. the shaded leaves and branches), by which we derived a mean T_{leaf} value for the sunlit leaves (e.g. Fig. S8d). Finally, we calculated ΔT using T_{leaf} minus T_{air} of the same time, which was generated by interpolating weather station records (see section *Environmental variables* above). Notably, the method of temperature measurements using FLIR-T650sc thermal camera have been cross-referenced with thermocouple measurements by multiple previous studies (e.g. Page *et al.*, 2018), and is regarded as an accurate method with comparable results as thermocouple measurements.

At the PE site, we selected 1-3 unshaded canopy-top leaves from different branches for T_{leaf} measurements. The measurements were taken using a hand-held infrared camera (870-1 Testo; Lenzkirch in Schwarzwald, Germany) at a 0.5 m distance directly above the leaves.

Thermal images were taken with a resolution of 640 × 480 pixels. These thermal images were acquired under clear-sky days between 10:30 am to 1:30 pm local time. To accurately obtain T_{leaf}, the thermal images and relevant measurement conditions (i.e. target distance and leaf emissivity of 0.95) were input to a professional software—Testo AG IRSoft 4.0 (Testo Ag, Lenzkirch, Germany) for further processing. The temperature measurements from the Testo thermal camera were cross-referenced using infrared point thermometer measurements (572-2 Fluke; Everett, WA, USA) and found to be consistent (Fig.S1 in Majcher, 2018). Mean T_{leaf} was derived as an average temperature recorded for all the pixels encompassed within the leaf margin (see Majcher, 2018). Finally, we calculated ΔT as a difference between T_{leaf} and same-time T_{air}, which came from the after-interpolated flux tower records.

Leaf width

At the CB, XSBN, and PE sites, we used leaf maximum width (cm) for leaf width, as it has been shown as a key biotic control of leaf boundary layer conductance (e.g. g_H in Equation 3), and thus importantly regulates ΔT variability (Campbell & Norman, 2012; Wright *et al.*, 2017). The leaf maximum width of the canopy-top sunlit leaves was measured following Majcher (2018). Specifically, leaves were harvested for leaf width measurements following a two-step approach. First is to obtain the images of leaf samples. At CB and XSBN, we used a Canon digital scanner (FSU201, Canon, Tokyo, Japan). Specifically, we placed each of sampled leaves on the panel of the scanner with known dimensions, flatten it with a white board, and scanned it for image records. At the PE site, we put each leave on a scaled board, flatten it with a transparent board, and then photographed it using a DSLR Camera (EOS XTi Canon, Tokyo, Japan). Second is to estimate the leaf maximum width. We used the ShapeFilter plugin (Wagner & Lipinski, 2013) in ImageJ Software (Schneider *et al.*, 2012) to extract and measure the maximum width of leaves.

Relevant references for Supporting Method 1

Campbell GS, Norman J. 2012. *An introduction to environmental biophysics*: Springer Science & Business Media.

Croft H, Chen JM, Luo X, Bartlett P, Chen B, Staebler RM. 2017. Leaf chlorophyll content as a proxy for leaf photosynthetic capacity. *Global Change Biology* **23**: 3513-3524.

de Boor Carl. 1978. *A Practical Guide to Splines*. Springer-Verlag, New York.

Féret JB, Gitelson A, Noble S, Jacquemoud S. 2017. PROSPECT-D: Towards modeling leaf optical properties through a complete lifecycle. *Remote Sensing of Environment* **193**: 204-215.

Majcher BM. 2018. *Leaf thermoregulation in the semi-arid tropics of Brazil.* Master thesis, Imperial College London.

Jacquemoud S, Baret F. 1990. PROSPECT: A model of leaf optical properties spectra. *Remote Sensing of Environment* **34**: 75-91.

Page, GF, Liénard JF, Pruett MJ, Moffett KB. 2018. Spatiotemporal dynamics of leaf transpiration quantified with time-series thermal imaging. *Agricultural and Forest Meteorology* **256**: 304-314.

Rogers A, Serbin SP, Ely KS, Sloan VL, Wullschleger SD. 2017. Terrestrial biosphere models underestimate photosynthetic capacity and CO_2 assimilation in the Arctic. *New Phytologist* **216**: 1090-1103.

Schneider CA, Rasband WS, Eliceiri KW. 2012. NIH Image to ImageJ: 25 years of image analysis. *Nature methods* **9**: 671-675.

Senior RA, Hill JK, Edwards DP. 2019. ThermStats: an R package for quantifying surface thermal heterogeneity in assessments of microclimates. *Methods in Ecology and Evolution* **10**: 1606-1614.

Shiklomanov AN, Dietze MC, Viskari T, Townsend PA, Serbin SP. 2016. Quantifying the influences of spectral resolution on uncertainty in leaf trait estimates through a Bayesian approach to RTM inversion. *Remote Sensing of Environment* **183**: 226-238.

Wagner T, Lipinski HG. 2013. IJBlob: an ImageJ library for connected component analysis and shape analysis. *Journal of Open Research Software.* doi.org/10.5334/jors.ae.

Wright IJ, Dong N, Maire V, Prentice IC, Westoby M, Díaz S, Gallagher RV, Jacobs BF, Kooyman R, Law EA et al. 2017. Global climatic drivers of leaf size. *Science* **357**: 917-921.

Wu J, Kobayashi H, Stark SC, Meng R, Guan K, Tran NN, Gao S, Yang W, Restrepo‐Coupe N, Miura T et al. 2018. Biological processes dominate seasonality of remotely sensed canopy greenness in an Amazon evergreen forest. *New Phytologist* **217**: 1507-1520.

Wu J, Rogers A, Albert LP, Ely K, Prohaska N, Wolfe BT, Oliveira Jr RC, Saleska SR, Serbin SP. 2019. Leaf reflectance spectroscopy captures variation in carboxylation

capacity across species, canopy environment and leaf age in lowland moist tropical forests. *New Phytologist* **224**: 663-674.

Wu J, Serbin SP, Ely KS, Wolfe BT, Dickman LT, Grossiord C, Michaletz ST, Collins AD, Detto M, McDowell NG et al. 2020. The response of stomatal conductance to seasonal drought in tropical forests. *Glob Chang Biology* **26**: 823-839.